Accepted Manuscript

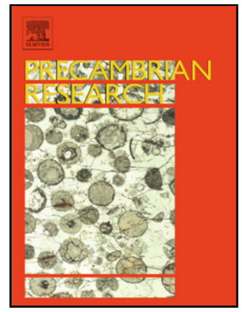

Title: Neoproterozoic crustal growth of the Southern Yangtze Block: Geochemical and zircon U–Pb geochronological and Lu-Hf isotopic evidence of Neoproterozoic diorite from the Ailaoshan zone

Author: Yongfeng Cai Yuejun Wang Peter A. Cawood Yuzhi Zhang Aimei Zhang

PII: S0301-9268(15)00148-5
DOI: http://dx.doi.org/doi:10.1016/j.precamres.2015.05.008
Reference: PRECAM 4258

To appear in: *Precambrian Research*

Received date: 24-1-2015
Revised date: 22-4-2015
Accepted date: 3-5-2015

Highlights

► Dioritic rocks in the Ailaoshan zone yield U-Pb ages of ~800 Ma.

► They derived from partial melting of mafic lower crust.

► They have been produced in a subduction-related tectonic setting.

► The igneous activity records the Neoproterozoic continental growth of SW Yangtze.

Neoproterozoic crustal growth of the Southern Yangtze Block: Geochemical and zircon U–Pb geochronological and Lu-Hf isotopic evidence of Neoproterozoic diorite from the Ailaoshan zone

Yongfeng Cai [1, 2], Yuejun Wang [2, *], Peter A. Cawood [3, 4], Yuzhi Zhang [2], Aimei Zhang [5]

1 College of Earth Sciences, Guilin University of Technology, Guilin, Guangxi 541004, China

2 School of Earth Science and Geological Engineering, Sun Yat-Sen University, Guangzhou 510275, China

3 Department of Earth Sciences, University of St Andrews, North Street, St Andrews KY16 9AL, UK

4 Centre for Exploration Targeting, School of Earth and Environment, University of Western Australia, 35 Stirling Highway, Crawley, WA 6009, Australia

5 Third Institute of Oceanography, State Oceanic Administration, Xiamen, 361005, China

* Corresponding author

Address: School of Earth Science and Geological Engineering
Sun Yat-Sen University
No. 135, Xingang Xi Road, Guangzhou, 510275
People's Republic of China
Tel: 86-20-84111209
Email: wangyuejun@mail.sysu.edu.cn

Abstract: Neoproterozoic felsic igneous rocks associated with mafic-ultramafic bodies along the margins of the Yangtze Block, South China, can be used to constrain the continental crustal growth and secular evolution of the region. LA-ICPMS zircon U-Pb dating of the Adebo quartz diorite pluton in the Ailaoshan tectonic zone on the southern margin of the Yangtze Block gives the Neoproterozoic age of 800 ± 7 Ma and εHf(t) values in the range of -1.03 to +3.75 with two-stage model age of 1.3-1.6 Ga. The pluton is characterized by relatively low SiO_2 (60.97-64.41 wt. %) and total alkalis (K_2O+Na_2O, 7.35-9.14 wt. %) and high Al_2O_3 content (16.98-18.21 wt. %) with mg-number of 36-39. REE-normalized patterns show enrichment in LREE with (La/Yb)cn of 11.36 to 19.77 and Europium negative anomalies with Eu/Eu*=0.61-0.74. The samples are characterized by negative Nb-Ta ((Nb/La)n = 0.18-0.35) and P, Ti, Sr anomalies and high Y concentrations (33.79-41.04 ppm) and low Sr/Y ratios (5.65-10.16). Their isotopic composition are similar to those of the Neoproterozoic mafic igneous rocks in the Ailaoshan zone and the southwestern Yangtze Block, indicating that the quartz diorite was produced by partial melting of mafic lower crust. The diorite also shows the similar geochemical characteristics with adakitic rocks from thickened lower crust or amphibolite and eclogite experimental melts. In combination with their arc-related geochemical signatures and synchronous developed adakitic rocks in the region, the Adebo quartz diorite pluton might be produced in a subduction-related tectonic setting during Neoproterozoic crustal growth along the margins of Yangtze Block.

Keywords: Quartz diorite; Neoproterozoic; Crustal growth; Petrogenesis; Ailaoshan zone; Yangtze Block

1. Introduction

It is well established that the Earth's continental crust has a bulk composition broadly resembles that of intermediate, subduction-related volcanic rocks (Cawood et al., 2013b; Davidson and Arculus, 2006; Rudnick and Fountain, 1995). Identifying the geodynamic controls on continental crust generation is fundamental to understanding the differentiation of the silicate Earth. A prevalent view holds that arc magmatism is the major mode of continent formation (Collins, 2002; Sengor et al., 1993; Taylor, 1967). However, a paradox argues that episodic crustal growth is ascribed to mantle plume and continent generation reflects deep-seated thermal anomalies rather than arc magmatism (Condie, 1998; Kemp et al., 2009; Stein and Hofmann, 1994). The subduction factory is just one of crustal recycling and differentiation rather than growth (Plank, 2005).

South China preserves a long record of Neoproterozoic igneous activity but the setting of this activity has considered to be geodynamically related to a variety of tectonic models including supra-subduction zone, plume and continental extension models (e.g., Li et al., 2003; Zhao and Zhou, 2007; Zheng et al., 2008; Wang et al., 2013b, 2014b). The felsic and mafic-ultramafic intrusive rocks in South China Block (SCB) are relatively well-studied (Fig. 1; Cawood et al., 2013a; Dong et al., 2011, 2012; Li et al., 2003; Wang et al., 2008a,b; Wang et al., 2013b, 2014b; Xu et al., 2014; Yao et al., 2014a, b; Zhang et al., 2013; Zhao and Cawood, 2012; Zheng et al., 2008; Zhou et al., 2002a, 2006b; Zhu et al., 2014). However, there is only limited geochemical and geochronological data for associated intermediate rocks, especially along the southern margin of the SCB. In this article, we explore the significance of arc-back-arc processes for crustal growth with reference to the Ailaoshan zone and by combining systematic geochemical, petrogenetic and zircon U-Pb-Hf isotopic data. Our goal is to (1) determine the timing of intrusion, (2) decipher the petrogenesis and nature of the magma source, and (3) discuss the Neoproterozoic setting and implications for crustal growth along the southern margin of the Yangtze Block.

2. Geological background and petrology

The Ailaoshan zone in SW Yunnan Province (South China) (Fig. 2a) extends over 300 km and is 20–30 km wide. It is bound by the Indochina Block to the southwest along the Anding-Jiujia Fault, by the SCB to the northeast along Red River Fault and links to the Jinshajiang orogenic belt to the northwest (Mo et al., 1993; Yunnan BGMR, 1983; Zhong, 1998; Zi et al., 2013). Southeast of the Ailaoshan zone are a variety of geological blocks in northern Vietnam and Laos, including the Song Hien and Song Da rifts, and the Truong Son and Loei fold belts, which are suggested to have affinities to the South China Craton and Indochina Block, respectively (e.g., Chung et al., 1997; Hanski et al., 2004; Lai et al., 2014).

The Ailaoshan zone consists of two NW-trending metamorphic belts including high-grade metamorphic belt to the northeast and low-grade metamorphic belt to the southwest, which are divided by the Ailaoshan Fault (Fig. 2a). Amphibolite to granulite facies rocks of the high-grade metamorphic belt were derived from protoliths of intermediate to basic volcanic rock and volcaniclastic sedimentary units (Lu, 1989). The greenschist-facies metamorphism belt is comprised of the Paleozoic and Mesozoic strata with minor Cenozoic sedimentary rocks, which have been folded and intruded by magmatic rocks (Yunnan BGMR, 1983; Zhong, 1998).

The Adebo quartz diorite pluton is located at the southeast part of the Ailaoshan zone, which intruded into the Proterozoic strata and were unconformably overlain by the Devonian clastic, argillaceous and carbonate sedimentary rocks (Fig. 2a,b). Samples from the Adebo quartz diorite pluton are gray, medium grained and mainly composed of plagioclase (~60%), hornblende (~25%), quartz (~10%) and K-feldspar (~5%), with a small amount of clinopyroxene, biotite magnetite, ilmenite, apatite and zircon (Fig. 3). Plagioclase is commonly subhedral with length of 0.5-1.0 mm, and partly altered to sericite and epidote. The hornblendes are subhedral to anhedral, and are commonly interstitial, sometimes poikilitic, enclosing plagioclase and oxides, and partly altered to chlorite and epidote. Quartz is anhedral and relatively fine-grained polygonal quartz aggregates. The interstitial quartz zones show the same optical orientation, engulfing hornblende or plagioclase. K-feldspar is mostly subhedral 0.5-1.5 mm, and is partly altered to kaolinite.

3. Analytical methods

Zircon grains were obtained for two representative samples (10HH-33A and 10HH-35A) by conventional heavy liquid and magnetic techniques. Zircons, together with standard 91500 were mounted in epoxy. Internal structure of grains was documented by transmitted and reflected light micrographs, along with cathodoluminescence (CL) images.

The zircon U-Pb isotopic results for sample 10HH-33A and 10HH-35A were analyzed with a VG PlasmaQuad Excell inductively coupled plasma-mass spectrometer (ICP-MS) equipped with a New Wave Research LUV213 laser ablation system at the University of Hong Kong. The laser ablation system has a beam of 213 nm UV light from a frequency-quintupled Nd:YAG laser. Analytical settings were a beam diameter of ca. 40 μm, a 10 Hz of repetition rate, and energy of 0.6 mJ to 1.3 mJ per pulse. The equipment was tuned with total U signals ranging from 3×10^4 to 100×10^4. Typical ablation time was 30 s to 60 s, leading to pits 20 μm to 40 μm deep. The detailed analytical procedure followed Xia et al. (2004). Data reduction was carried out using the Isoplot/Ex v. 3 program (Ludwig, 2001). The U-Pb dating results for 10HH-33A and 10HH-35A are listed in Table 1.

In-situ Lu-Hf isotopic analyses were performed by the LA-MC-ICPMS method using a Thermo Finnigan Neptune multicollector-ICPMS and a Geolas CQ 193 nm laser ablation system housed at the Institute of Geology and Geophysics, Chinese Academy of Sciences, Beijing, China. Hf isotopic data reported in this study were obtained from the same zircon grains for which the U-Pb data was also determined. Detailed descriptions for the analytical techniques are described by (Wu et al., 2006a). Although Lu-Hf isotopes were measured on the same spots used for U-Pb dating to minimize zoning effects, the laser ablation size was ~50–65 μm, slightly larger than that of preexisting pits (~30 μm), made by the U–Pb dating. The external analytical error of the method is about 4ε unit (Wu et al., 2006a). Hf isotope results are reported with a 2σ error in Table 2.

Representative samples for the whole-rock elemental and isotopic analyses were pulverizing to 200-mesh. Major oxides were analyzed at the State Key Laboratory of Isotope Geochemistry, Guangzhou Institute of Geochemistry (GIG), CAS by a wavelength X-ray fluorescence spectrometry using a Rigaku ZSX100e spectrometer with the relative standard derivations of < 5%. Trace element contents were measured using Perkin-Elmer Sciex ELAN 6000 inductively coupled plasma-mass spectrometer (ICP-MS) at the GIG, CAS. Detailed sample preparation and analytical procedure followed Qi et al. (2000). The analytical results of major oxides and elements are shown in Table 3.

4. Results

4.1. Zircon U–Pb geochronology

Zircons separated from samples 10HH-33A and 10HH-35A are mainly euhedral to subhedral with length between 100 and 150 μm and have aspect ratios ranging from 2:1 to 4:1. The CL images exhibit weakly oscillatory zoning with variable luminescence, indicative of an igneous origin (Fig. 4a-b). The zircon U-Pb dating results are listed in Table 1 and shown in Fig. 4.

Sample 10HH-33A is located to west of Adebo (Fig. 2b). Twenty-five grains were analyzed, which exhibit a relatively wide range of U and Th concentrations with U = 138-2139 ppm, Th = 56-579 ppm and Th/U ratios mostly are in the range of 0.40 to 0.95 (Table 1). Five analyses deviate from concordia, indicating a function of late Pb loss. Twenty spots yield a coherent group with the $^{206}Pb/^{238}U$ weighted mean age of 799 ± 10 Ma with MSWD = 0.13 (Fig. 4a), interpreted as the crystallization age of the sample.

Sample 10HH-35A is taken from south of Adebo (Fig. 2b). Twenty-five analytical grains were carried out on this sample. Their U and Th concentrations range from 162 to 746 ppm and 98 to 377 ppm, respectively, and Th/U ratios from 0.30 to

0.85. Two spots deviate from concordia, suggestive of Pb loss during later metamorphism. Twenty-three spots yield a $^{206}Pb/^{238}U$ weighted mean age of 800 ± 9 Ma with MSWD = 0.11 (Fig. 4b), representing the formation age of the sample.

Two samples are indistinguishable in age within error and combining the data from two samples yields an age of 800 ± 7 Ma (n = 43, MSWD = 0.10).

4.2. Geochemical characteristics

Representative samples from the Adebo quartz diorite have 60.97-64.41 wt. % of SiO_2, 0.71-0.78 wt. % of TiO_2, 16.98-18.21 wt. % of Al_2O_3 and 2.27-3.05 wt. % of CaO (Fig. 5). They show mg-number of 36-39. Their K_2O contents range from 1.22 wt. % to 4.34 wt. % and Na_2O from 4.34 wt. % to 6.13 wt. % and can be classfied as alkali-calcic series (Fig. 5b). On Harker variation diagrams (Fig. 6a-h), MgO, FeOt, and Al_2O_3 correlate negatively with SiO_2, whereas TiO_2 and P_2O_5 are relative constant irrespective of SiO_2. The others major oxides show some degree of scattering, suggests that the compositional variations are not a simple reflection of the fractional crystallization of the magma, and may in part reflect metamorphic alteration of samples.

REE-normalized and multi-element primitive mantle-normalized patterns have (La/Yb)cn = 11.36-19.77, (Gd/Yb)cn = 1.84-2.57, and moderate negative Europium anomalies with Eu/Eu* = 0.61-0.74 (Fig. 7a). They are enrichment in large ion lithophile elements (LILEs) and characterized by negative Nb-Ta ((Nb/La)n =0.18-0.35) and P, Ti, Sr anomalies (Fig. 7b) and high Y concentration (33.79-41.04 ppm) and low Sr/Y ratios (5.65-10.16).

4.3. Zircon in-situ Lu-Hf isotopes

Twenty-three analyses on sample 10HH-33A have $^{176}Lu/^{177}Hf$ ratios ranging from 0.000392 to 0.001779 and present-day $^{176}Hf/^{177}Hf$ ratios from 0.282257 to 0.282364 with initial $^{176}Hf/^{177}Hf$ ratios vary from 0.282244 to 0.282337. εHf(t) values range from -1.03 to +2.28 with two-stage model ages (T_{DM2}) from 1.4 G to 1.6 Ga (Table 2). Twenty-four analyses on zircons from sample 10HH-35A have $^{176}Lu/^{177}Hf$

and present-day $^{176}Hf/^{177}Hf$ ratios in the range of 0.000448 to 0.002646 and 0.282305 to 0.282393, respectively. Initial $^{176}Hf/^{177}Hf$ ratios range from 0.282294 to 0.282379, and εHf(t) values from +0.76 to +3.75 with model age of 1.3-1.5 Ga.

5. Discussion

5.1. Alteration effects and fractional crystallization processes

Loss on ignition (LOI) for samples from Adebo quartz diorite are low at less than 2.14 wt. %. High field strength elements, such as Th, Ti, Nb, Ta, Zr, Hf, Y and REEs and Nd isotopic compositions, are generally considered immobile during alteration or weathering processes (Barnes et al., 1985; Wang et al., 2013a). Zr is usually selected to test the mobility of other incompatible elements (Rolland et al., 2009). Our samples display positive correlation between Zr and Th, La, Yb, Nd and Ti (no shown). These signatures, together with the subparallel REE and multi-element patterns in figure 7a-b, indicate that these HFSEs and REEs elements can represent their original compositions during metamorphism and hydrothermal alteration.

Rocks from Adebo quartz diorite pluton show a general fractional crystallization trend indicated by decreasing MgO, FeOt, Al_2O_3, Cr and Ni concentrations (Fig. 6). These trends can be interpreted as fractionation of amphibole, Fe-Ti-oxides and plagioclase. The negative Eu and Sr anomaly (Fig. 7a-b) suggests that plagioclase may play a major role during fractional crystallization. P_2O_5 is relative constant irrespective of SiO_2, indicative of no obvious fractionation of apatite. Fractionation between LREE and HREE can also monitor fractional crystallization processes. Depletion of HREE, together with enrichment of LREE during fractional crystallization, is compatible with fractionation of amphibole, which tends to concentrate the HREE.

5.2. Petrogenesis of the dioritic rocks

The continental crust has an overall andesitic composition, with a vertical stratification from mafic lower crust to more evolved granite-dominated upper crust (e.g., Annen et al., 2006; Cawood et al., 2013b; Condie and Kröner, 2013; Zhou et al., 2014, 2015). Thus, the genesis of intermediate to silicic magmatic rocks is key point to understanding the evolution of the continental crust. There are currently three popular models for the generation of intermediate rocks, as follows: (i) partial melting of harzburgite in the mantle wedge, modified by fluids or melts liberated from a subducting slab (e.g., Carmichael, 2002; Parman and Grove, 2004; Tatsumi, 1982); (ii) fractional crystallization of mantle-derived magma in shallow crustal magma chambers or in the deep crust at or close to the Moho (e.g. Arth and Hanson, 1972; Kushiro, 1969; Osborn, 1969; Shaw et al., 1993); and (iii) dehydration partial melting of the lower mafic crust (e.g. Flierdt et al., 2003; Jung et al., 2002; Watters, 1978), with or without mixing between silicic magmas and mafic magmas (e.g. Annen et al., 2006; Cantagrel et al., 1984; Clemens and Vielzeuf, 1987; Gao et al., 2004).

Intermediate rocks, such as diorite produced in the mantle wedge or by the differentiation of mantle-derived magmas, have elevated MgO contents and high mg-numbers, a requirement for equilibrium with the Mg-rich olivine (e.g., Grove et al., 2003; Tatsumi, 1982), whereas typical “normal diorites” with low mg-numbers could not have been in equilibrium with mantle rocks (e.g., Annen et al., 2006, Rahman, 2013). The Adebo quartz diorite contains low Cr, Ni and mg-numbers, which are incompatible with either a primitive or evolved original mafic melt, suggesting they were not generated from partial melting of refractory mantle wedge or differentiation of mantle-derived magmas. Fractional crystallization model additionally reveal that removal of 80% mafic minerals from the mantle-derived parental magma would raise Th contents to 3.0 ppm (Rapp and Watson, 1995). The Adebo quartz diorite has high Th concentrations (7.47-17.82 ppm), significantly higher than 3.0 ppm, against origin from high-degrees fractional crystallization of mafic magmas.

An alternative model for generating the Adebo quartz diorite involving partial melting of mafic lower crust is based on the following geological evidence. (1) MgO values and mg-numbers for the quartz diorite are similar to adakitic rocks sourced from thickened lower crust or those of amphibolite and eclogite experimental melts at high pressures of 1.0-4.0 GPa (Figs. 6e and 8a-b). (2) Magmatic rocks produced by fractional crystallization always show continuous compositional trends from basaltic rocks originated from mantle to felsic rocks originated from residual magmas (e.g., Litvinovsky et al., 2002; Roberts et al., 2000). However, the Adebo quartz diorite exhibits compositional trends that differ from those of the mafic rocks in Ailaoshan zone (Fig. 6). Additionally, they have a compositional trend that does not correspond with the fractional crystallization trends of plagioclase, hornblende and garnet (Fig. 9). These geochemical characteristics suggest that they were not generated by fractional crystallization of mantle-derived magma. (3) The quartz diorite has relatively high $\varepsilon_{Hf}(t)$ values (−1.03 to +3.75) with two-stage model ages of 1.32 Ga to 1.56 Ga (Table 2), different from those of basement rocks in South China Block, which lacks Mesoproterozoic rocks (apart from Hainan Island), implying that they could not have originated from basement rocks in the SCB (Liu et al., 2014). (4) They have Hf isotopic compositions that are similar to those of Neoproterozoic mafic rocks in the Ailaoshan zone (Cai et al., 2014; Qi et al., 2012) (Fig. 10). Such similarities are consistent with the quartz diorites being derived from Neoproterozoic (~815 Ma) underplated mafic magma in the lower curst. (5) This model is supported by the presence of Neoproterozoic (826–750 Ma) diorites (Zhao et al., 2010), adakitic rocks (Zhao et al., 2008a; Zhao and Zhou, 2007) and granitoids (Chen et al., 2014; Wang et al., 2014a; Zhao et al., 2013) along the western, northern and eastern margins of the Yangtze Block that are considered to be derived from mafic lower crust or juvenile arc crust. On the basis of above considerations, it is herein proposed that the Adebo quartz diorites were likely produced by partial melting of juvenile mafic lower crust.

Sill-like intrusions are commonly considered to be a major component of mid- to lower crustal regions (Bohlen, 1987), and numerical modelling suggests they do not need to be very thick to melt mafic lower crust (Petford and Gallagher, 2001). Experimental evidence indicates that dehydrating melting of mafic intrusions newly emplaced into the lower crust can generate massive silicic magmas, particularly in regions with high heat flow (Beard and Lofgren, 1991; Rapp and Watson, 1995; Rapp et al., 1991; Roberts and Clemens, 1993; Wolf and Wyllie, 1994). The existence of Neoproterozoic mafic rocks (Cai et al., 2014; Qi et al., 2012) in Ailaoshan zone implies that the Neoproterozoic mafic magmatism provides the heat necessary to melt mafic lower crust.

The concentration of Al_2O_3 can be used to estimate pressure (Rapp and Watson, 1995; Rapp et al., 1991). At <1.6 GPa, the experimental melts have low than 15 wt. % Al_2O_3 (low-Al_2O_3 partial melt) and amphibole, plagioclase and orthopyroxene are residual phases. The Al_2O_3 concentration of melts is >15 wt. % if the pressure is >1.6 GPa, and the resulting restite composed of amphibole, plagioclase, clinopyroxene and garnet. At 2.0–3.0 GPa, the melt is in equilibrium with a plagioclase-absent, garnet-bearing amphibolite, eclogite or granulite. These experimental results further reveal that the partial melts at highest pressure conditions should have the highest Sr concentrations and Sr/Y ratios, but the lowest Y and HREEs concentrations (Petford and Atherton, 1996). The Adebo quartz diorite has geochemical features that are similar to those of the partial melts derived from basaltic rocks (Fig. 8). They have SiO_2 contents of 60.97-64.41 wt. %, Al_2O_3 contents of 16.98-18.21 wt. %, K_2O/Na_2O ratios of 0.2-0.97 and high LREEs concentrations relative to HREEs (Fig. 7a), and those with the lower Y concentrations of 33.79 ppm have the higher Sr/Y ratios of 10.16. These characteristics would be expected for partial melts from a basaltic protolith, most likely a garnet-bearing amphibolite at pressures of >1.6 GPa. A garnet-bearing amphibolite residue for Adebo quartz diorite coincides with the low Rb/Sr and K/Rb ratios and HREEs concentrations (Fig. 6a).

The majority of the Adebo quartz dioritic samples has K_2O >3.5 wt. %, CaO >6 wt. %, TiO_2 <1.0 wt. % and mg-number of greater than 37. Such characteristics are only obtained by experiments performed between 1000-1100 °C (Jung et al., 2002). In the plots proposed by Rapp and Watson (1995), all the samples fall into the field of high-temperature melting (1000 to 1100 °C) at high pressures (Figs. 6a and g). Therefore, it is possible that the Adebo quartz diorite was produced at relatively high-temperature. On the other hand, the Adebo quartz diorite shows slightly enrichment in TiO_2 and MgO, and low Na_2O and CaO concentrations compared with the experimental melts of alkali basalts (e.g., Jung et al., 2002; Rapp and Watson, 1995). They have relatively high K_2O abundances compared with the experimental melts of low-K Archean greenstone and low-K olivine tholeiite (Rapp and Watson, 1995), suggestive of K-rich source for the Adebo quartz diorites. In addition, the geochemical compositions for the Adebo quartz diorite are similar to those of the experimental melts derived from high-Al basalts (Rapp and Watson, 1995). Thus, the protolith of the Adebo quartz diorite was possibly high-Al, K-rich, calcic basalts. Such geochemical characteristics of the basaltic protolith are typically exemplified by mantle-derived rocks in active continental margins (Miyashiro, 1974). Furthermore, the Adebo quartz diorite has low concentrations of Ni and Cr, depletion of HFSE (e.g. Nb, Ta) and enrichment of LILE (e.g., Rb, Ba, K), similar with those least evolved members of some island arc tholeiite and calc-alkaline series (e.g. Perfit et al., 1980). Enrichment of LILE might be caused by transfer of volatiles from dehydrating subducted oceanic crust to the mantle wedge (e.g. Gribble et al., 1998; Leat et al., 2000; Woodhead et al., 1993).

In summary, the Adebo quartz diorite was most likely generated by dehydration melting of basalt at relatively high temperature and moderate pressure in the lower crust, and their protolith was modified by subduction components.

5.3. Implication for Neoproterozoic arc-related magmatism and crustal growth

Neoproterozoic felsic rocks associated with mafic-ultramafic to intermediate plutons are widespread along the northern and western margins of the Yangtze Block, e.g., the Xixiang, Bikou, Kangding and Yanbian groups (Fig. 1). These rocks range in age from ca. 865 Ma to ca. 710 Ma and include mafic to silicic igneous rocks and associated volcaniclastic rocks with the geochemical indicators of a convergent plate setting (e.g. Dong et al., 2012; Druschke et al., 2006; Qi et al., 2012; Sun et al., 2009; Wang et al., 2012; Yan et al., 2004; Zhao and Zhou, 2007, 2008, 2009; Zhao et al., 2010, 2011, 2013; Zhou et al., 2002a,b, 2006a,b).

Our study for Adebo quartz diorite pluton in the Ailaoshan zone yields the zircon U-Pb ages of 800 ± 7 Ma, implying the presence of the Neoproterozoic magmatism along the southwest Yangtze Block. Cai et al. (2014) proposed that plagioclase amphibolites with ages of ~815-800 Ma in this zone represented a back-arc extension of the supra-subduction zone magmatism along the western margin of the Yangtze Block. In addition, arc related igneous rocks from the southern margin of the Yangtze Block include 769 ± 7 Ma hornblende-gabbro and 761 ± 11 Ma adakitic granodiorite (Qi et al., 2012) and 843-770 Ma gneisses from the Diancangshan region (Lin et al., 2012; Liu et al., 2008) in the Ailaoshan zone, and 760-751 Ma granitic rocks in the PoSen complex in northern Vietnam (Wang et al., 2011).

Generation of the high temperatures (ca. 1000 to 1100 °C) for forming the Adebo quartz diorite by dehydration melting of the basaltic rock in the lower crust is required for significant heat input through underplating by mantle-derived magmas (e.g., Clemens, 1990; Vielzeuf et al., 1990). Active subduction with associated magmatic underplating along southwest Yangtze Block provides a likely source for heating and melting of the lower crustal rocks. Subsequent magmas were emplaced into the upper crust undergoing fractional crystallization to form the Adebo quartz diorite which records a phase of Neoproterozoic crustal growth along the western margin of the Yangtze Block.

5. Conclusions

In the Ailaoshan zone, southwestern Yangtze Block, middle-Neoproterozoic (ca. 800 Ma) Adebo quartz diorite pluton has relatively low SiO_2 and mg-number and high Al_2O_3 contents. The quartz diorite is characterized by enrichment of LILEs, HFSEs, LREEs and negative Nb-Ta anomalies. Major and trace element compositions, zircon U-Pb ages and Hf isotope data imply that the quartz diorites were generated by partial melting of mafic lower crust. Neoproterozoic subduction may have triggered the crust and mantle-derived magmatism observed in the Ailaoshan zone. This igneous activity along with consanguineous activity along the western and northern margins of the Yangtze Block records a phase of Neoproterozoic continental growth.

Acknowledgements This study was supported by National Natural Science Foundation of China (41190073 and 41372198), National Basic Research Program of China (2014CB440901), Basic Operation Expense of Sun Yat-Sen University and Startup Foundation for Doctors of Guilin University of Technology (002401003475). We thank X-P Xia, T-P Peng, F Guo, L-Y Ma and F-F Zhang for their help during fieldwork and dating analyses.

References

Annen, C., Blundy, J.D., Sparks, R.S.J., 2006. The genesis of intermediate and silicic magmas in deep crustal hot zones. Journal of Petrology 47, 505-539.

Arth, J.G., Hanson, G.N., 1972. Quartz diorites derived by partial melting of eclogite or amphibolite at mantle depths. Contributions to Mineralogy and Petrology 37, 161-174.

Barnes, S.J., Naldrett, A.J., Gorton, M.P., 1985. The origin of the fractionation of Platinum-Group elements in Terrestrial Magmas. Chemical Geology 53, 303-323.

Beard, J.S., Lofgren, G.E., 1991. Dehydration melting and water-saturated melting of basaltic and andesitic greenstones and amphibolites at 1, 3, and 6. 9 kb. Journal of Petrology 32, 365-401.

Bohlen, S.R., 1987. Pressure-temperature-time paths and a tectonic model for the evolution of granulites. Journal of Geology 95, 617-632.

Cai, Y.F., Wang, Y.J., Cawood, P.A., Fan, W.M., Liu, H.C., Xing, X.W., Zhang, Y.Z., 2014. Neoproterozoic subduction along the Ailaoshan zone, South China: geochronological and geochemical evidence from amphibolite. Precambrian Research 245, 13-28.

Cantagrel, J.M., Didier, J., Gourgaud, A., 1984. Magma mixing: origin of intermediate rocks and “enclaves” from volcanism to plutonism. Physics of the Earth and Planetary Interiors 35, 63-76.

Carmichael, I.S., 2002. The andesite aqueduct: perspectives on the evolution of intermediate magmatism in west-central (105–99°W) Mexico. Contributions to Mineralogy and Petrology 143, 641-663.

Cawood, P.A., Hawkesworth, C.J., Dhuime, B., 2013b. The continental record and the generation of continental crust. Geological Society of America Bulletin 125, 14-32.

Cawood , P.A., Wang , Y.J., Xu , Y.J., Zhao, G.C., 2013a. Locating South China in Rodinia and Gondwana : a fragment of greater India lithosphere? Geology 41, 903-906.

Chen, X., Wang, D., Wang, X.L., Gao, J.F., Shu, X.J., Zhou, J.C., Qi, L., 2014. Neoproterozoic chromite-bearing high-Mg diorites in the western part of the Jiangnan orogen, southern China: geochemistry, petrogenesis and tectonic implications. Lithos 200-201, 35-48.

Chung, S.L., Lee, T.Y., Lo, C.H., Wang, P.L., Chen, C.Y., Yem, N.T., Hoa, T.T., Wu, G.Y., 1997. Intraplate extension prior to continental extrusion along the Ailao Shan Red River shear zone. Geology 25, 311-314.

Clemens, A., 1990. The granulite-granite connection. In: Vielzeuf, D., Vidal, P. (Eds.), Granulites and Crustal Evolution. Dordrecht, Kluwer, pp. 25-36.

Clemens, J.D., Vielzeuf, D., 1987. Constraints on melting and magma production in the crust. Earth and Planetary Science Letters 86, 287-306.

Collins, W.J., 2002. Hot orogens, tectonic switching and the creation of continental crust. Geology 30, 535-538.

Condie, K.C., 1998. Episodic continental growth and supercontinents: a mantle avalanche connection? Earth and Planetary Science Letters 163, 97-108.

Condie, K.C., Kröner, A., 2013. The building blocks of continental crust: evidence for a major change in the tectonic setting of continental growth at the end of the Archean. Gondwana Research 23, 394-402.

Davidson, J.P., Arculus, R.J., 2006. The significance of Phanerozoic arc magmatism in generating continental crust. In: Brown, M., Rushmer, T. (Eds.), Evolution and Differentiation of the Continental Crust. Cambridge University Press, Cambridge, pp. 135-172.

Depaolo, D.J., 1981. Trace-element and isotopic effects of combined wallrock assimilation and fractional crystallization. Earth and Planetary Science Letters 53, 189-202.

Dong, Y.P., Liu, X.M., Santosh, M., Chen, Q., Zhang, X.N., Li, W., He, D.F., Zhang, G.W., 2012. Neoproterozoic accretionary tectonics along the northwestern margin of the Yangtze Block, China: constraints from zircon U-Pb geochronology and geochemistry. Precambrian Research 196, 247-274.

Dong, Y.P., Liu, X.M., Santosh, M., Zhang, X.N., Chen, Q., Yang, C., Yang, Z., 2011. Neoproterozoic subduction tectonics of the northwestern Yangtze Block in South China: constrains from zircon U-Pb geochronology and geochemistry of mafic intrusions in the Hannan Massif. Precambrian Research 189, 66-90.

Druschke, P., Andrew, D.H., Yan, Q.R., Wang, Z.Q., Wang, T., 2006. Stratigraphic and U–Pb SHRIMP Detrital Zircon evidence for a Neoproterozoic Continental Arc, Central China: Rodinia implications. Journal of Geology 114, 627-636.

Du, L.L., Guo, J.H., Nutman, A.P., Wyman, D., Geng, Y.S., Yang, C.H., Liu, F.L., Ren, L.D., Zhou, X.W., 2014. Implications for Rodinia reconstructions for the initiation of Neoproterozoic subduction at ~860 Ma on the western margin of the Yangtze Block: evidence from the Guandaoshan Pluton. Lithos 196–197, 67-82.

Flierdt, T.V.D., Hoernes, S., Jung, S., Masberg, P., Hoffer, E., Schaltegger, U., Friedrichsen, H., 2003. Lower crustal melting and the role of open-system processes in the genesis of syn-orogenic quartz diorite-granite-leucogranite associations: constraints from Sr-Nd-O isotopes from the Bandombaai Complex, Namibia. Lithos 67, 205-226.

Gao, S., Rudnick, R.L., Yuan, H.L., Liu, X.M., Liu, Y.S., Xu, W.L., Ling, W.L., Ayers, J., Wang, X.C., Wang, Q.H., 2004. Recycling lower continental crust in the North China craton. Nature 432, 892-897.

Gribble, R.F., Stern, R.J., Newman, S., Bloomer, S.H., O'Hearn, T., 1998. Chemical and isotopic composition of lavas from the Northern Mariana Trough: implications for magmagenesis in back-arc basins. Journal of Petrology 39, 125-154.

Griffin, W.L., Pearson, N.J., Belousova, E., Jackson, S.E., van Achterbergh, E., O'Reilly, S.Y., Shee, S.R., 2000. The Hf isotope composition of cratonic mantle: LAM-MC-ICPMS analysis of zircon megacrysts in kimberlites. Geochimica et Cosmochimica Acta 64, 133-147.

Grove, T.L., Elkins-Tanton, L.T., Parman, S.W., Chatterjee, N., Muntener, O., Gaetani, G.A., 2003. Fractional crystallization and mantle-melting controls on calc-alkaline differentiation trends. Contributions to Mineralogy and Petrology 145, 515-533.

Hanski, E., Walker, R., Huhma, H., Polyakov, G., Balykin, P., Tran Trong, H., Ngo Thi, P., 2004. Origin of the Permian-Triassic komatiites, northwestern Vietnam. Contributions to Mineralogy and Petrology 147, 453-469.

Jung, S., Hoernes, S., Mezger, K., 2002. Synorogenic melting of mafic lower crust: constraints from geochronology, petrology and Sr, Nd, Pb and O isotope geochemistry of quartz diorites (Damara orogen, Namibia). Contributions to Mineralogy and Petrology 143, 551-566.

Kemp, A. I. S., Hawkesworth, C. J., Collins, W. J., Cray, C. M., Blevin, P. L., 2009. Isotopic evidence for rapid continental growth in an extensional accretionary orogen: The Tasmanides, eastern Australia. Earth and Planetary Science Letters 284, 455-466.

Kushiro, I., 1969. System Forsterite-Diopside-Silica with and without Water at High Pressures. Americal Journal of Science 267, 269-294.

Lai, C.K., Meffre, S., Crawford, A.J., Zaw, K., Xue, C.D., Halpin, J.A., 2014. The Western Ailaoshan Volcanic Belts and their SE Asia connection: a new tectonic model for the Eastern Indochina Block. Gondwana Research 26, 52-74.

Leat, P.T., Livermore, R.A., Millar, I.L., Pearce, J.A., 2000. Magma supply in back-arc spreading centre segment e2, east Scotia Ridge. Journal of Petrology 41, 845-866.

Li, Z.X., Li, X.H., Kinny, P.D., Wang, J., Zhang, S., Zhou, H., 2003. Geochronology of Neoproterozoic syn-rift magmatism in the Yangtze Craton, South China and correlations with other continents: evidence for a mantle superplume that broke up Rodinia. Precambrian Research 122, 85-109.

Lin, T.H., Chung, S.L., Chiu, H.Y., Wu, F.Y., Yeh, M.W., Searle, M.P., Iizuka, Y., 2012. Zircon U-Pb and Hf isotope constraints from the Ailao Shan-Red River shear zone on the tectonic and crustal evolution of southwestern China. Chemicla Geology 291, 23-37.

Litvinovsky, B.A., Jahn, B.M., Zanvilevich, A.N., Shadaev, M.G., 2002. Crystal fractionation in the petrogenesis of an alkali monzodiorite-syenite series: the Oshurkovo plutonic sheeted complex, Transbaikalia, Russia. Lithos 64, 97-130.

Liu, C.H., Zhao, G.C., Liu, F.L., Shi, J.R., 2014. Zircon U-Pb and Lu-Hf isotopic and whole-rock geochemical constraints on the provenance and age of the Shuangshanzi and Qinglonghe Groups in Eastern Hebei: implications for the tectonic evolution of the Eastern Block. Precambrian Research 255(2): 699-715.

Liu, J.B., Zhang, L.M., 2013. Neoproterozoic low to negative δ18O volcanic and intrusive rocks in the Qinling Mountains and their geological significance. Precambrian Research, 230(0), 138-167.

Liu, J.L., Wang, A.J., Cao, S.Y., Zou, Y.X., Tang, Y., Chen, Y., 2008. Geochronology and tectonic implication of migmatites from Diancangshan, western Yunnan, China. Acta Petrologica Sinica 24, 413–420 (in Chinese with English abstract).

Lu, L.Z., 1989. The metamorphic series and crustal evolution of the basement of the Yangtze platform. Journal of Southeast Asian Earth 3, 293–301.

Ludwig, K.R., 2001. Users manual for Isoplot/Ex rev. 2.49. Berkeley Geochronology Centre Special Publication. No. 1a, 56 pp.

Miyashiro, A., 1974. Volcanic rock series in island arcs and active continental margins. Americal Journal of Science 274, 321-355.

Mo, X.X., Lu, F.X., Shen, S.Y., 1993. Sanjiang Tethyan volcanism and related mineralization. . Geological Publishing House, Beijing, pp. 178–235.

Osborn, E.F., 1969. The complementariness of orogenic andesite and alpine peridotite. Geochimica et Cosmochimica Acta 33, 307-324.

Parman, S.W., Grove, T.L., 2004. Harzburgite melting with and without H_2O:

experimental data and predictive modeling. Journal of Geophysical Research: Solid Earth 109, B02201.

Perfit, M.R., Gust, D.A., Bence, A.E., Arculus, R.J., Taylor, S.R., 1980. Chemical characteristics of island-arc basalts: implications for mantle sources. Chemical Geology 30, 227-256.

Petford, N., Atherton, M., 1996. Na-rich partial melts from newly underplated basaltic crust: the Cordillera Blanca Batholith, Peru. Journal of Petrology 37, 1491-1521.

Petford, N., Gallagher, K., 2001. Partial melting of mafic (amphibolitic) lower crust by periodic influx of basaltic magma. Earth and Planetary Science Letters 193, 483-499.

Plank, T., 2005. Constraints from thorium/lanthanum on sediment recycling at subduction zones and the evolution of continents. Journal of Petrology 46, 921-944.

Qi, L., Hu, J., Gregoire, D.C., 2000. Determination of trace elements in granites by inductively coupled plasma mass spectrometry. Talanta 51, 507-513.

Qi, X.X., Zeng, L.S., Zhu, L.H., Hu, Z.C., Hou, K.J., 2012. Zircon U-Pb and Lu-Hf isotopic systematics of the Daping plutonic rocks: implications for the Neoproterozoic tectonic evolution of the northeastern margin of the Indochina block, Southwest China. Gondwana Research 21, 180-193.

Rahman, E.A., 2013. Geochemistry of island arc dolerites and diorites along Qift–Quseir asphaltic road, central Eastern Desert, Egypt. Arab J Geosci, 1-12.

Rapp, R.P., 1995. Amphibole-out phase boundary in partially melted metabasalt, its control over liquid fraction and composition, and source permeability. Journal of Geophysical Research: Solid Earth 100, 15601-15610.

Rapp, R.P., Watson, E.B., 1995. Dehydration melting of metabasalt at 8-32 Kbar: implications for continental growth and crust-mantle recycling. Journal of Petrology 36, 891-931.

Rapp, R.P., Watson, E.B., Miller, C.F., 1991. Partial melting of amphibolite/eclogite and the origin of Archean trondhjemites and tonalites. Precambrian Research 51,

1-25.
Roberts, M.P., Clemens, J.D., 1993. Origin of high-potassium, talc-alkaline, I-type granitoids. Geology 21, 825-828.
Roberts, M.P., Pin, C., Clemens, J.D., Paquette, J.L., 2000. Petrogenesis of mafic to felsic plutonic rock associations: the calc-alkaline Querigut Complex, French Pyrenees. Journal of Petrology 41, 809-844.
Rolland, Y., Galoyan, G., Bosch, D., Sosson, M., Corsini, M., Fornari, M., Verati, C., 2009. Jurassic back-arc and Cretaceous hot-spot series In the Armenian ophiolites: implications for the obduction process. Lithos 112, 163-187.
Rudnick, R.L., Fountain, D.M., 1995. Nature and composition of the continental crust: a lower crustal perspective. Review of Geophysics 33, 267-309.
Sen, C., Dunn, T., 1994. Dehydration melting of a basaltic composition amphibolite at 1.5 and 2.0 Gpa: implications for the origin of adakites. **Contributions to Mineralogy and Petrology** 117, 394-409.
Sengor, A.M.C., Natal'in, B.A., Burtman, V.S.,1993. Evolution of the Altaid tectonic collage and Palaeozoic crustal growth in Eurasia. Nature 364, 299-307.
Shaw, A., Downes, H., Thirlwall, M.F., 1993. The quartz-diorites of Limousin: elemental and isotopic evidence for Devono-Carboniferous subduction in the Hercynian Belt of the French Massif-Central. Chemical Geology 107, 1-18.
Sinclair, J.A., 2001. Petrology, geochemistry, and geochronology of the “Yanbian ophiolite suite”, South China: implications for the western extension of the Sibao Orogen. Honours Thesis, The University of Western Australia, Perth, 69 pp.
Sisson, T.W., Ratajeski, K., Hankins, W.B., Glazner, A.F., 2005. Voluminous granitic magmas from common basaltic sources. **Contributions to Mineralogy and Petrology** 148, 635-661.
Springer, W., Seck, H.A., 1997. Partial fusion of basic granulites at 5 to 15 kbar: implications for the origin of TTG magmas. **Contributions to Mineralogy and Petrology** 127, 30-45.
Stein, M., Hofmann, A.W., 1994. Mantle plumes and episodic crustal growth. Nature

372, 63-68.

Stern, C.R., Kilian, R., 1996. Role of the subducted slab, mantle wedge and continental crust in the generation of adakites from the Andean Austral Volcanic Zone. **Contributions to Mineralogy and Petrology** 123, 263-281.

Sun, S.S., McDonough, W.F., 1989. Chemical and isotopic systematics of oceanic basalts: implications for mantle composition and processes. Geological Society, London, Special Publications 42, 313-345.

Sun, W.H., Zhou, M.F., Gao, J.F., Yang, Y.H., Zhao, X.F., Zhao, J.H., 2009. Detrital zircon U–Pb geochronological and Lu–Hf isotopic constraints on the Precambrian magmatic and crustal evolution of the western Yangtze Block, SW China. Precambrian Research 172, 99-126.

Tatsumi, Y., 1982. Origin of high-magnesian andesites in the Setouchi Volcanic Belt, Southwest Japan 2: melting phase-relations at high-pressures. Earth and Planetary Science Letters 60, 305-317.

Taylor, S.R., 1967. The origin and growth of continents. Tectonophysics 4, 17-34.

Vielzeuf, D., Clemens, J.D., Pin, C., Moinet, E., 1990. Granites, granulites, and crustal differentiation. In: Vielzeuf, D., Vidal, P. (Eds.), Granulites and Crustal Evolution. Nato ASI Series C-311. Kluwer, Dordrecht, pp. 59-85.

Wang, P.L., Lo, C.H., Lan, C.Y., Chung, S.L., Lee, T.Y., Tran, N.N., Sano, Y., 2011. Thermochronology of the PoSen complex, northern Vietnam: implications for tectonic evolution in SE Asia. Journal of Asian Earth Science 40, 1044-1055.

Wang, Q., McDermott, F., Xu, J.F., Bellon, H., Zhu, Y.T., 2005. Cenozoic K-rich adakitic volcanic rocks in the Hohxil area, northern Tibet: lower-crustal melting in an intracontinental setting. Geology 33, 465-468.

Wang, Q., Wyman, D.A., Li, Z.X., Bao, Z.W., Zhao, Z.H., Wang, Y.X., Jian, P., Yang, Y.H., Chen, L.L., 2010. Petrology, geochronology and geochemistry of ca. 780 Ma A-type granites in South China: petrogenesis and implications for crustal growth during the breakup of the supercontinent Rodinia. Precambrian Research 178, 185-208.

Wang, X.C., Li, X.H., Li, W.X., Li, Z.X., Liu, Y., Yang, Y.H., Liang, X.R., Tu, X.L., 2008b. The Bikou basalts in the northwestern Yangtze block, South China: remnants of 820-810 Ma continental flood basalts? Geological Society of America Bulletin 120, 1478-1492.

Wang, X.L., Shu, L.S., Xing, G.F., Zhou, J.C., Tang, M., Shu, X.J., Qi, L., Hu, Y.H., 2012. Post-orogenic extension in the eastern part of the Jiangnan orogen: evidence from ca 800-760 Ma volcanic rocks. Precambrian Research 222, 404-423.

Wang, X.L., Zhao, G.C., Zhou, J.C., Liu, Y.S., Hu, J., 2008a. Geochronology and Hf isotopes of zircon from volcanic rocks of the Shuangqiaoshan Group, South China: implications for the Neoproterozoic tectonic evolution of the eastern Jiangnan orogen. Gondwana Research 14, 355-367.

Wang, X.L., Zhou, J.C., Griffin, W.L., Zhao, G.C., Yu, J.H., Qiu, J.S., Zhang, Y.J., Xing, G.F., 2014a. Geochemical zonation across a Neoproterozoic orogenic belt: isotopic evidence from granitoids and metasedimentary rocks of the Jiangnan orogen, China. Precambrian Research 242, 154-171.

Wang, Y.J., Zhang, A.M., Cawood, P.A., Fan, W.M., Xu, J.F., Zhang, G.W., Zhang, Y.Z., 2013b. Geochronological, geochemical and Nd-Hf-Os isotopic fingerprinting of an early Neoproterozoic arc-back-arc system in South China and its accretionary assembly along the margin of Rodinia. Precambrian Research 231, 343-371.

Wang, Y.J., Zhang, A.M., Fan, W.M., Zhang, Y.H., Zhang, Y.Z., 2013a. Origin of paleosubduction-modified mantle for Silurian gabbro in the Cathaysia Block: Geochronological and geochemical evidence. Lithos 160, 37-54.

Wang, Y.J, Zhang, Y.Z., Fan, W.M., Geng, H.Y, Zou, H.P., Bi, X.W., 2014b. Early Neoproterozoic accretionary assemblage in the Cathaysia Block: Geochronological, Lu–Hf isotopic and geochemical evidence from granitoid gneisses. Precambrian Research 249, 144-161.

Watters, W.A., 1978. Diorite and Associated Intrusive and Metamorphic Rocks between Port William and Paterson Inlet, Stewart Island, and on Ruapuke Island. New Zeal Journal of Geology and Geophylogy 21, 423-442.

Wolf, M.B., Wyllie, P.J., 1994. Dehydration-melting of amphibolite at 10 kbar: the effects of temperature and time. **Contributions to Mineralogy and Petrology** 115, 369-383.

Woodhead, J., Eggins, S., Gamble, J., 1993. High-field strength and transition element systematics in island-arc and back-arc basin basalts: evidence for multiphase melt extraction and a depleted mantle wedge. Earth and Planetary Science Letters 114, 491-504.

Wu, F.Y., Yang, Y.H., Xie, L.W., Yang, J.H., Xu, P., 2006a. Hf isotopic compositions of the standard zircons and baddeleyites used in U–Pb geochronology. Chemical Geology 234, 105-126.

Wu, R.X., Zheng, Y.F., Wu, Y.B., Zhao, Z.F., Zhang, S.B., Liu, X.M., Wu, F.Y., 2006b. Reworking of juvenile crust: element and isotope evidence from Neoproterozoic granodiorite in South China. Precambrian Research 146, 179-212.

Xia, X.P., Sun, M., Zhao, G.C., Li, H.M., Zhou, M.F., 2004. Spot zircon U-Pb isotope analysis by ICP-MS coupled with a frequency quintupled (213 nm) Nd-YAG laser system. Geochemical Journal 38, 191-200.

Xu, X.B., Xue, D.J., Li, Y., Hu, P., Chen, N.S., 2014. Neoproterozoic sequences along the Dexing–Huangshan fault zone in the eastern Jiangnan orogen, South China: geochronological and geochemical constrains. Gondwana Research 25, 368-382.

Yan, Q.R., Hanson, A.D., Wang, Z.Q., Druschke, P.A., Yan, Z., Wang, T., Liu, D.Y., Song, B., Pan, P., Zhou, H., Jiang, C.F., 2004. Neoproterozoic subduction and rifting on the northern margin of the Yangtze Plate, China: implications for Rodinia reconstruction. International Geology Review 46, 817-832.

Yao, J.L., Shu, L.S., Santosh, M., 2014a. Neoproterozoic arc-trench system and breakup of the South China Craton: constraints from N-MORB type and arc-related mafic rocks, and anorogenic granite in the Jiangnan orogenic belt. Precambrian Research 247, 187-207.

Yao, J.L., Shu, L.S., Santosh, M., Zhao, G.C., 2014b. Neoproterozoic arc-related mafic–ultramafic rocks and syn-collision granite from the western segment of the Jiangnan Orogen, South China: constraints on the Neoproterozoic assembly of the Yangtze and Cathaysia Blocks. Precambrian Research 243, 39-62.

Yunnan BGMR, 1983. Bureau of geology and mineral resources of Yunnan: Geological Map of Yunnan, scale 1:1 000000. Kumming.

Zhang, Y.Z., Wang, Y.J., Geng, H.Y., Zhang, Y.H., Fan, W.M., Zhong, H., 2013. Early Neoproterozoic (similar to 850 Ma) back-arc basin in the Central Jiangnan Orogen (Eastern South China): geochronological and petrogenetic constraints from meta-basalts. Precambrian Research 231, 325-342.

Zhao, G.C., Cawood, P.A., 2012. Precambrian geology of China. Precambrian Research 222, 13-54.

Zhao, J.H., Zhou, M.F., 2007. Neoproterozoic adakitic plutons and arc magmatism along the western margin of the Yangtze Block, South China. Journal of Geology 115, 675-689.

Zhao, J.H., Zhou, M.F., 2008. Neoproterozoic adakitic plutons in the northern margin of the Yangtze Block, China: partial melting of a thickened lower crust and implications for secular crustal evolution. Lithos 104, 231-248.

Zhao, J.H., Zhou, M.F., 2009. Melting of newly formed mafic crust for the formation of Neoproterozoic I-Type granite in the Hannan Region, South China. Journal of Geology 117, 54-70.

Zhao, J.H., Zhou, M.F., Yan, D.P., Yang, Y.H., Sun, M., 2008a. Zircon Lu–Hf isotopic constraints on Neoproterozoic subduction-related crustal growth along the western margin of the Yangtze Block, South China. Precambrian Research 163, 189-209.

Zhao, J.H., Zhou, M.F., Yan, D.P., Zheng, J.P., Li, J.W., 2011. Reappraisal of the ages of Neoproterozoic strata in South China: no connection with the Grenvillian orogeny. Geology 39, 299-302.

Zhao, J.H., Zhou, M.F., Zheng, J.P., 2013. Neoproterozoic high-K granites produced by melting of newly formed mafic crust in the Huangling region, South China. Precambrian Research 233, 93-107.

Zhao, J.H., Zhou, M.F., Zheng, J.P., Fang, S.M., 2010. Neoproterozoic crustal growth and reworking of the Northwestern Yangtze Block: constraints from the Xixiang dioritic intrusion, South China. Lithos 120, 439-452.

Zhao, X.F., Zhou, M.F., Li, J.W., Wu, F.Y., 2008b. Association of Neoproterozoic A- and I-type granites in South China: implications for generation of A-type granites in a subduction-related environment. Chemical Geology 257, 1-15.

Zheng, Y.F., Wu, R.X., Wu, Y.B., Zhang, S.B., Yuan, H.L., Wu, F.Y., 2008. Rift melting of juvenile arc-derived crust: geochemical evidence from Neoproterozoic volcanic and granitic rocks in the Jiangnan Orogen, South China. Precambrian Research 163, 351-383.

Zheng, Y.F., Zhang, S.B., Zhao, Z.F., Wu, Y.B., Li, X.H., Li, Z.X., Wu, F.Y., 2007. Contrasting zircon Hf and O isotopes in the two episodes of Neoproterozoic granitoids in South China: implications for growth and reworking of continental crust. Lithos 96, 127-150.

Zhong, D.L., 1998. Paleotethysides in western Yunnan and Sichuan, China. Science Press, Beijing, pp. 9-215.

Zhou, M.F., Kennedy, A.K., Sun, M., Malpas, J., Lesher, C.M., 2002a. Neoproterozoic arc-related mafic intrusions along the northern margin of South China: implications for the accretion of Rodinia. Journal of Geology 110, 611-618.

Zhou, M.F., Ma, Y.X., Yan, D.P., Xia, X.P., Zhao, J.H., Sun, M., 2006b. The Yanbian terrane (Southern Sichuan Province, SW China): a Neoproterozoic arc assemblage in the western margin of the Yangtze block. Precambrian Res 144, 19-38.

Zhou, M.F., Yan, D.P., Kennedy, A.K., Li, Y.Q., Ding, J., 2002b. SHRIMP U-Pb zircon geochronological and geochemical evidence for Neoproterozoic arc-magmatism along the western margin of the Yangtze Block, South China. Earth and Planetary Science Letters 196, 51-67.

Zhou, M.F., Yan, D.P., Wang, C.L., Qi, L., Kennedy, A., 2006a. Subduction-related origin of the 750 Ma Xuelongbao adakitic complex (Sichuan Province, China):

implications for the tectonic setting of the giant Neoproterozoic magmatic event in South China. Earth and Planetary Science Letters 248, 286-300.

Zhou, Y., Liang, X., Liang, X., Jiang, Y., Wang, C., Fu, J., Shao, T., 2014. U–Pb geochronology and Hf-isotopes on detrital zircons of Lower Paleozoic strata from Hainan Island: New clues for the early crustal evolution of southeastern South China, Gondwana Research doi:10.1016/j.gr.2014.01.015.

Zhou, Y., Liang, X., Wu, S., Cai, Y., Liang, X., Shao, T., Wang, C., Fu, J., Jiang, Y., 2015. Isotopic geochemistry, zircon U–Pb ages and Hf isotopes of A-type granites from the Xitian W–Sn deposit, SE China: Constraints on petrogenesis and tectonic significance, Journal of Asian Earth Science 105, 122-139.

Zhu, X.Y., Chen, F.K., Nie, H., Siebel, W.G., Yang, Y.Z., Xue, Y.Y., Zhai, M.G., 2014. Neoproterozoic tectonic evolution of South Qinling, China: evidence from zircon ages and geochemistry of the Yaolinghe volcanic rocks. Precambrian Research 245, 115-130.

Zi, J.W., Cawood, P.A., Fan, W.M., Tohver, E., Wang, Y.J., McCuaig, T.C., Peng, T.P., 2013. Late Permian-Triassic Magmatic Evolution in the Jinshajiang Orogenic Belt, SW China and Implications for Orogenic Processes Following Closure of the Paleo-Tethys. Americal Journal of Science 313, 81-112.

Figure Caption

Fig.1. Simplified geotectonic map showing the Ailaoshan zone (modified after Lin et al., 2012; Zhao and Cawood, 2012). Abbreviation: G=Group, (G)=Granite, (B)=Basalt, (S)=Schist. The cited geochronological data are from Cai et al. (2014).

Fig.2. Schematic geological map of the Ailaoshan zone with showing the Adebo quartz diorite pluton in western Yunnan Province.

Fig.3. Microscope photographs for the Adebo quartz diorite along the Ailaoshan zone. (a) 10HH-33A, (b) 10HH-35A. Pl: plagioclase, Amp: amphibole, Qz: quartz, Cpx: clinopyroxene.

Fig.4. Zircon U–Pb concordia diagrams for the Adebo quartz diorite along the Ailaoshan zone. (a) Sample 10HH-33A from the western Adebo pluton, and (b) sample 10HH-35A from the southern Adebo pluton.

Fig.5. Plots of (a) Zr/TiO_2 versus SiO_2, and (b) SiO_2 versus K_2O+Na_2O-CaO for the Adebo quartz diorite pluton along the Ailaoshan zone. Abbreviation: YB=Yangtze Block. Data for the diorite from northwestern YB are from Zhao et al. (2010), Liu and Zhang (2013) and Dong et al. (2012). High-K granites from central YB are from Zhao et al. (2013). Mafic rocks from Ailaoshan zone are from Cai et al. (2014) and references therein. Gabbro-diorites from western YB are from Du et al. (2014), Sinclair (2001) and Li et al. (2003).

Fig.6. Plots of SiO_2 versus (a) MgO, (b) Fe_2O_3T, (c) Al_2O_3, (d) CaO, (e) K_2O, (f) Na_2O, (g) TiO_2, and (h) P_2O_5 for the Adebo quartz diorite pluton along the Ailaoshan zone. The fields of metabasaltic and eclogite experimental melts are from Rapp and Watson (1995); Sisson et al. (2005); Springer and Seck (1997) and references therein.

Fig.7. Chondrite-normalized REE patterns (a) and primitive mantle-normalized incompatible trace element spidergrams (b) for the Adebo quartz diorite pluton along the Ailaoshan zone. The normalized values for the chondrite and primitive mantle are from (Sun and McDonough, 1989). Abbreviation:

YB=Yangtze Block. Data for the diorites from northwestern YB are from Zhao et al. (2010), Liu and Zhang (2013), Dong et al. (2012), diorites in eastern YB from Chen et al. (2014) and references therein, and gabbro-diorites in western YB from Du et al. (2014), Sinclair (2001) and Li et al. (2003).

Fig.8. Plots of (a) MgO versus SiO_2, and (b) mg-number versus SiO_2 (Wang et al., 2005) for the Adebo quartz diorite pluton along the Ailaoshan zone. The fields of metabasaltic and eclogite experimental melts (1.0−4.0 GPa), pure crustal partial melts at 0.8−1.6 GPa and 1000−1050 °C and at 0.7 GPa and 825−950 °C are from Rapp (1995); Rapp and Watson (1995); Sen and Dunn (1994); Sisson et al. (2005); Springer and Seck (1997) and references therein. Curve for mantle AFC was calculated based on Depaolo (1981) with a mass-assimilation/ fractionation ratio of r=2, reflecting a relatively hot mantle wedge, and 80% amphibole + 20% clinopyroxene as fractionating phases (after Stern and Kilian, 1996).

Fig.9. Plots of SiO_2 versus (a) Eu/Eu*, (b) Sr/Sr*, (c) Zr/Sm, and (d) Dy/Yb for the Adebo quartz diorite pluton along the Ailaoshan zone. Abbreviation: YB=Yangtze Block. Data for the diorite from northwestern YB are from Zhao et al. (2010), Liu and Zhang (2013), Dong et al. (2012). High-K granites from central YB are from Zhao et al. (2013), mafic rocks in the Ailaoshan zone from Cai et al. (2014) and references therein, and gabbro-diorite in western YB from Du et al. (2014), Sinclair (2001) and Li et al. (2003).

Fig.10. Schematic diagram for zircon U–Pb age (Ma) versus εHf(t) from igneous rocks around the Yangtze Block. The line denotes the evolution of depleted mantle (DM) with a present-day $^{176}Hf/^{177}Hf$ = 0.28325 and $^{176}Lu/^{177}Hf$ = 0.0384 (Griffin et al., 2000). The Hf isotope data for the igneous rocks are from Wu et al. (2006b); Zheng et al. (2007, 2008); Wang et al. (2010); Zhao and Zhou (2007, 2009); Zhao et al. (2008a,b, 2010) and references therein.

Table Caption

Table 1 LA-ICP-MS zircon U-Pb isotopic analyses of the representative quartz diorite along the Ailaoshan zone

Table 2 Zircon in-situ Lu-Hf isotopic compositions for the Adebo quartz diorite along the Ailaoshan zone

Table 3 Major element (wt %) and trace element (ppm) compositions of the Adebo quartz diorite

Table 1 LA-ICP-MS zircon U-Pb isotopic analyses of the representative quartz diorite along the Ailaoshan zone

Spot	Element(ppm)		Th/U	Isotope ratio						Age (Ma)			
	^{232}Th	^{238}U		^{207}Pb/^{206}Pb	±1σ	^{207}Pb/^{235}U	±1σ	^{206}Pb/^{238}U	±1σ	^{207}Pb/^{206}Pb	±1σ	^{206}Pb/^{238}U	±1σ
10HH-33A quartz diorite, western Adebo, Yunnan (LA-ICPMS method)													
10HH-33A-01	148	2139	0.07	0.0639	0.002	1.1745	0.043	0.1317	0.004	739	38	797	23
10HH-33A-02	138	338	0.41	0.0668	0.003	1.0512	0.051	0.1131	0.004	831	96	691	21
10HH-33A-03	273	422	0.65	0.0655	0.002	1.1952	0.044	0.1316	0.004	791	72	797	21
10HH-33A-04	133	333	0.40	0.0684	0.003	1.1236	0.048	0.1189	0.003	880	91	724	20
10HH-33A-05	282	512	0.55	0.0660	0.002	1.2165	0.049	0.1323	0.004	806	64	801	21
10HH-33A-06	145	268	0.54	0.0644	0.002	1.1716	0.051	0.1319	0.004	754	79	799	21
10HH-33A-07	183	343	0.53	0.0664	0.002	1.2148	0.056	0.1318	0.004	820	76	798	20
10HH-33A-08	255	439	0.58	0.0681	0.003	1.2395	0.071	0.1314	0.004	872	96	796	23
10HH-33A-09	243	397	0.61	0.0635	0.002	1.1774	0.051	0.1330	0.004	724	67	805	20
10HH-33A-10	241	318	0.76	0.0723	0.004	1.3317	0.085	0.1318	0.005	995	112	798	26
10HH-33A-11	244	422	0.58	0.0630	0.003	1.1575	0.053	0.1325	0.004	709	98	802	23
10HH-33A-12	99	225	0.44	0.0648	0.003	1.1767	0.049	0.1317	0.004	769	85	798	22
10HH-33A-13	150	306	0.49	0.0672	0.003	0.9945	0.052	0.1070	0.004	856	108	655	21

10HH-33A-14	579	613	0.94	0.0644	0.004	1.1645	0.061	0.1322	0.004	754	122	800	23
10HH-33A-15	196	347	0.56	0.0634	0.003	1.1765	0.051	0.1326	0.004	722	92	803	22
10HH-33A-16	148	240	0.62	0.0629	0.003	1.1522	0.056	0.1319	0.004	702	106	798	25
10HH-33A-17	274	464	0.59	0.0630	0.003	1.1706	0.055	0.1320	0.004	706	89	799	24
10HH-33A-18	211	326	0.65	0.0685	0.003	1.2547	0.047	0.1317	0.004	883	-119	798	21
10HH-33A-19	137	251	0.55	0.0669	0.003	1.2347	0.063	0.1316	0.004	835	134	797	23
10HH-33A-20	122	224	0.55	0.0640	0.003	1.1810	0.049	0.1324	0.004	743	88	802	21
10HH-33A-21	443	469	0.95	0.0599	0.003	1.1037	0.053	0.1321	0.004	611	100	800	24
10HH-33A-22	222	334	0.67	0.0655	0.002	1.2036	0.052	0.1316	0.004	791	79	797	20
10HH-33A-23	127	264	0.48	0.0680	0.003	1.2470	0.056	0.1321	0.004	878	83	800	21
10HH-33A-24	56	138	0.40	0.0684	0.005	1.0088	0.070	0.1076	0.004	881	157	659	25
10HH-33A-25	161	535	0.30	0.0679	0.002	1.0776	0.053	0.1133	0.003	865	76	692	18
10HH-35A quartz diorite, southern Adebo, Yunnan (LA-ICPMS method)													
10HH-35A-01	241	477	0.51	0.0622	0.002	1.1310	0.038	0.1317	0.004	683	74	798	21
10HH-35A-02	224	463	0.48	0.0653	0.002	1.1983	0.039	0.1325	0.004	783	67	802	21
10HH-35A-03	234	391	0.60	0.0625	0.002	1.1510	0.039	0.1330	0.004	700	73	805	21
10HH-35A-04	159	304	0.52	0.0659	0.003	1.2083	0.055	0.1325	0.004	806	85	802	24

10HH-35A-05	377	746	0.51	0.0651	0.002	1.1843	0.044	0.1316	0.004	789	76	797	23
10HH-35A-06	123	234	0.53	0.0640	0.003	1.1556	0.048	0.1313	0.004	743	88	795	22
10HH-35A-07	144	316	0.46	0.0656	0.003	1.1938	0.059	0.1314	0.004	792	106	796	22
10HH-35A-08	137	206	0.67	0.0644	0.002	1.1782	0.047	0.1323	0.004	767	75	801	21
10HH-35A-09	251	418	0.60	0.0661	0.003	1.2167	0.058	0.1326	0.004	809	88	803	23
10HH-35A-10	306	511	0.60	0.0660	0.002	1.0514	0.045	0.1147	0.004	806	77	700	21
10HH-35A-11	228	500	0.46	0.0628	0.002	1.1545	0.040	0.1327	0.004	702	69	803	21
10HH-35A-12	292	675	0.43	0.0639	0.002	1.1732	0.038	0.1322	0.004	739	264	801	20
10HH-35A-13	193	332	0.58	0.0631	0.002	1.1530	0.045	0.1329	0.004	722	82	804	24
10HH-35A-14	98	328	0.30	0.0634	0.002	1.1457	0.044	0.1317	0.004	720	282	798	21
10HH-35A-15	246	510	0.48	0.0629	0.002	1.1566	0.039	0.1328	0.004	706	72	804	21
10HH-35A-16	118	241	0.49	0.0656	0.003	1.2071	0.069	0.1320	0.005	794	110	799	26
10HH-35A-17	102	162	0.63	0.0665	0.003	1.2066	0.057	0.1319	0.004	822	98	799	24
10HH-35A-18	209	344	0.61	0.0641	0.002	1.1771	0.049	0.1329	0.004	746	86	804	23
10HH-35A-19	102	265	0.38	0.0636	0.002	1.1523	0.045	0.1313	0.004	731	78	795	22
10HH-35A-20	238	468	0.51	0.0657	0.003	1.1988	0.059	0.1316	0.004	796	89	797	22
10HH-35A-21	248	638	0.39	0.0645	0.002	1.1760	0.042	0.1320	0.004	767	61	799	21

10HH-35A-22	174	313	0.56	0.0657	0.002	1.1901	0.048	0.1315	0.004	798	77	797	21
10HH-35A-23	221	410	0.54	0.0681	0.005	1.0528	0.066	0.1123	0.004	872	146	686	26
10HH-35A-24	347	409	0.85	0.0629	0.003	1.1437	0.058	0.1316	0.004	706	94	797	22
10HH-35A-25	233	396	0.59	0.0672	0.003	1.2310	0.065	0.1324	0.005	843	80	802	26

Table 2 Zircon in-situ Lu-Hf isotopic compositions for the Adebo quartz diorite along the Ailaoshan zone

Spot no.	$^{176}Yb/^{177}Hf$	2σ	$^{176}Lu/^{177}Hf$	2σ	$^{176}Hf/^{177}Hf$	2σ	$^{176}Hf/^{177}Hf(i)$	$\varepsilon_{Hf}(t)$	2σ	T_{DM1} (Ma)	T_{DM2}(Ma)
10HH-33A quartz diorite, western Adebo, Yunnan											
10HH-33A 02	0.020861	0.000553	0.000768	0.000019	0.282301	0.000023	0.282290	0.60	0.8	1335	1480
10HH-33A 03	0.034283	0.001614	0.001192	0.000055	0.282294	0.000018	0.282276	0.12	0.6	1360	1503
10HH-33A 04	0.020675	0.000853	0.000804	0.000033	0.282346	0.000028	0.282334	2.17	1.0	1273	1401
10HH-33A 05	0.023207	0.000251	0.000848	0.000008	0.282257	0.000019	0.282244	-1.03	0.7	1400	1560
10HH-33A 06	0.033013	0.000683	0.001189	0.000027	0.282274	0.000021	0.282256	-0.59	0.7	1388	1539
10HH-33A 07	0.029768	0.001307	0.001065	0.000045	0.282283	0.000019	0.282267	-0.22	0.7	1372	1520
10HH-33A 08	0.022963	0.001863	0.000805	0.000062	0.282313	0.000020	0.282301	1.01	0.7	1319	1459
10HH-33A 09	0.024085	0.000243	0.000863	0.000008	0.282320	0.000018	0.282307	1.20	0.6	1312	1450
10HH-33A 10	0.050058	0.001746	0.001779	0.000065	0.282364	0.000024	0.282337	2.28	0.8	1282	1396
10HH-33A 11	0.034392	0.000656	0.001211	0.000020	0.282298	0.000020	0.282280	0.24	0.7	1356	1498
10HH-33A 12	0.013853	0.000932	0.000527	0.000033	0.282298	0.000017	0.282290	0.60	0.6	1331	1480
10HH-33A 13	0.037110	0.001299	0.001637	0.000062	0.282321	0.000020	0.282296	0.83	0.7	1338	1468
10HH-33A 14	0.034499	0.002074	0.001235	0.000069	0.282339	0.000019	0.282320	1.67	0.7	1299	1426

10HH-33A 16	0.041688	0.001539	0.001450	0.000053	0.282303	0.000021	0.282281	0.28	0.7	1358	1496
10HH-33A 17	0.028094	0.000710	0.001016	0.000024	0.282297	0.000018	0.282281	0.30	0.6	1350	1495
10HH-33A 18	0.033202	0.000392	0.001177	0.000015	0.282262	0.000023	0.282244	-1.02	0.8	1405	1560
10HH-33A 19	0.034180	0.001321	0.001222	0.000048	0.282336	0.000021	0.282318	1.59	0.7	1302	1430
10HH-33A 20	0.029374	0.000555	0.001046	0.000020	0.282300	0.000020	0.282284	0.40	0.7	1347	1489
10HH-33A 21	0.023635	0.001610	0.000876	0.000056	0.282333	0.000019	0.282320	1.65	0.7	1295	1427
10HH-33A 22	0.036648	0.002213	0.001332	0.000079	0.282273	0.000020	0.282253	-0.70	0.7	1395	1544
10HH-33A 23	0.017510	0.000268	0.000653	0.000009	0.282315	0.000021	0.282305	1.15	0.7	1312	1452
10HH-33A 24	0.009666	0.000279	0.000392	0.000007	0.282304	0.000019	0.282298	0.88	0.7	1319	1466
10HH-33A 25	0.024673	0.000363	0.000926	0.000013	0.282261	0.000021	0.282247	-0.93	0.7	1397	1556
10HH-35A quartz diorite, southern Adebo, Yunnan											
10HH-35A 02	0.025338	0.000838	0.000921	0.000029	0.282346	0.000019	0.282332	2.10	0.7	1278	1405
10HH-35A 03	0.030236	0.001391	0.001071	0.000045	0.282331	0.000020	0.282315	1.49	0.7	1304	1435
10HH-35A 04	0.028112	0.001104	0.000992	0.000037	0.282340	0.000021	0.282326	1.86	0.7	1288	1417
10HH-35A 05	0.072106	0.003462	0.002646	0.000106	0.282393	0.000024	0.282354	2.86	0.8	1269	1367
10HH-35A 06	0.017220	0.000908	0.000620	0.000032	0.282315	0.000021	0.282305	1.15	0.7	1311	1452
10HH-35A 07	0.019923	0.001104	0.000750	0.000040	0.282390	0.000022	0.282379	3.75	0.8	1211	1323

10HH-35A 08	0.032142	0.000545	0.001120	0.000019	0.282346	0.000021	0.282329	1.97	0.7	1285	1411
10HH-35A 09	0.028728	0.000658	0.001022	0.000021	0.282335	0.000022	0.282319	1.64	0.8	1297	1428
10HH-35A 10	0.034943	0.001193	0.001256	0.000043	0.282319	0.000022	0.282300	0.96	0.8	1327	1461
10HH-35A 11	0.024927	0.000056	0.000921	0.000003	0.282321	0.000020	0.282307	1.19	0.7	1314	1450
10HH-35A 12	0.027680	0.000276	0.001031	0.000010	0.282320	0.000019	0.282304	1.11	0.7	1319	1454
10HH-35A 13	0.014485	0.001048	0.000536	0.000034	0.282305	0.000019	0.282297	0.85	0.7	1322	1467
10HH-35A 14	0.011589	0.000450	0.000448	0.000016	0.282328	0.000019	0.282322	1.73	0.7	1286	1424
10HH-35A 15	0.025279	0.000128	0.000937	0.000004	0.282347	0.000020	0.282333	2.11	0.7	1278	1404
10HH-35A 16	0.025304	0.000415	0.000890	0.000012	0.282308	0.000025	0.282295	0.78	0.9	1329	1470
10HH-35A 17	0.033231	0.001124	0.001185	0.000034	0.282313	0.000027	0.282295	0.79	0.9	1333	1470
10HH-35A 18	0.018649	0.001251	0.000688	0.000042	0.282309	0.000025	0.282298	0.90	0.9	1322	1464
10HH-35A 19	0.013358	0.000115	0.000511	0.000004	0.282343	0.000024	0.282336	2.22	0.8	1268	1399
10HH-35A 20	0.023407	0.001490	0.000888	0.000054	0.282382	0.000025	0.282369	3.39	0.9	1227	1341
10HH-35A 21	0.028179	0.000850	0.001104	0.000033	0.282344	0.000024	0.282327	1.93	0.9	1287	1413
10HH-35A 22	0.023503	0.000091	0.000834	0.000003	0.282309	0.000023	0.282297	0.85	0.8	1326	1467
10HH-35A 23	0.014443	0.000658	0.000656	0.000032	0.282340	0.000029	0.282330	2.01	1.0	1278	1409
10HH-35A 24	0.055042	0.000920	0.001883	0.000030	0.282323	0.000026	0.282294	0.76	0.9	1345	1472

10HH-35A	25	0.017977	0.000487	0.000668	0.000018	0.282323	0.000028	0.282313	1.41	1.0	1302	1439

Table 3 Major element (wt %) and trace element (ppm) compositions of the Adebo quartz diorite

Sample	10HH-33A	10HH-33B	10HH-33C	10HH-33D	10HH-35A	10HH-35C	10HH-35F	10HH-35G	10HH-35H
SiO_2	64.41	61.52	62.15	60.97	63.14	61.78	62.85	63.97	61.59
TiO_2	0.73	0.71	0.72	0.71	0.78	0.72	0.77	0.77	0.74
Al_2O_3	17.69	18.21	17.83	18.18	16.98	17.78	17.35	17.43	17.33
$Fe_2O_3^T$	4.76	5.37	5.15	5.32	5.44	5.03	4.84	4.95	5.18
MgO	1.14	1.38	1.40	1.46	1.45	1.39	1.28	1.24	1.32
CaO	2.98	2.87	2.82	3.05	2.77	2.27	2.83	2.65	2.69
K_2O	1.22	3.54	3.84	3.35	3.87	4.34	3.58	3.96	3.69
Na_2O	6.13	5.52	5.19	5.79	4.39	4.47	4.42	4.34	4.83
MnO	0.03	0.03	0.03	0.03	0.07	0.07	0.07	0.07	0.07
P_2O_5	0.23	0.24	0.23	0.24	0.19	0.18	0.19	0.19	0.18
L.O.I	1.03	1.24	1.08	1.19	1.08	2.14	1.11	1.08	1.85
Total	100.35	100.63	100.44	100.29	100.17	100.17	99.29	100.66	99.47
Mg#	35.88	37.46	38.78	39.01	38.33	39.10	38.13	36.86	37.26
Sc	7.33	6.73	7.03	6.83	9.375	8.909	8.74	9.382	8.923

Ti	4197.8	4013.1	4056.3	3984.7	4315.4	4057	4269.9	4324.7	4021
V	62.67	65.69	69.23	58.37	54.02	50.32	57.31	54.13	50.65
Cr	2.443	2.836	2.419	3.136	0.322	1.035	0.52	0.318	1.642
Co	6.809	6.622	7.146	6.854	7.89	7.115	7.88	7.78	7.116
Ni	5.679	6.226	5.439	6.637	0.918	2.178	1.064	0.924	3.186
Ga	23.19	23.59	23.52	23.68	22.7	23.25	23.12	22.64	23.24
Rb	50.19	66.32	58.96	71.43	109.3	134.3	105.3	110.4	135.6
Sr	218.8	291.2	247.8	343.2	326.6	261.6	356.7	331.2	265.5
Y	38.73	35.34	36.94	33.79	41.04	34.94	38.91	40.87	34.97
Zr	346.3	329.9	337.5	321.7	392.6	384.3	375.1	391.1	356.8
Nb	16.78	16.53	16.81	16.01	17.06	16.29	17.15	17.12	16.23
Cs	6.409	6.714	6.853	7.073	2.086	3.075	1.972	2.094	3.081
Ba	551	594	521	612	1260.7	1421.7	1175.6	1257.4	1423.2
La	48.68	53.22	46.67	58.95	67.62	84.84	92.33	67.58	84.86
Ce	100.6	108.1	101.3	118.1	126.8	155.6	173.94	126.6	155.4
Pr	12.47	15.82	13.28	14.86	15.04	17.16	19.82	15.12	17.14
Nd	48.47	54.92	50.12	49.94	54.96	59.87	66.72	55.02	59.85

Sm	9.191	10.223	10.374	10.623	9.286	9.56	10.22	10.293	9.79
Eu	2.108	2.237	2.163	2.312	1.829	1.93	1.931	1.833	1.95
Gd	8.462	9.075	8.564	8.491	8.13	8.185	8.839	8.15	8.191
Tb	1.325	1.382	1.308	1.264	1.209	1.171	1.223	1.211	1.182
Dy	7.184	6.933	7.036	6.752	7.014	6.532	6.964	7.012	6.541
Ho	1.352	1.284	1.313	1.163	1.42	1.214	1.376	1.45	1.221
Er	3.499	3.276	3.368	3.012	3.685	3.154	3.621	3.696	3.162
Tm	0.476	0.461	0.463	0.451	0.543	0.475	0.539	0.539	0.481
Yb	2.982	2.923	2.946	2.956	3.659	3.086	3.638	3.661	3.079
Lu	0.464	0.459	0.461	0.463	0.59	0.468	0.579	0.61	0.471
Hf	7.923	7.164	7.015	7.101	9.056	8.471	8.781	9.062	8.969
Ta	0.738	0.731	0.726	0.729	0.931	0.927	0.919	0.932	0.932
Th	7.466	11.281	9.942	9.324	13.84	16.82	16.13	17.82	16.78
U	2.215	2.273	2.234	2.197	4.161	3.399	4.184	4.158	3.411
∑REE	247.26	270.31	249.37	279.34	301.79	353.25	391.74	302.78	353.32

Figures

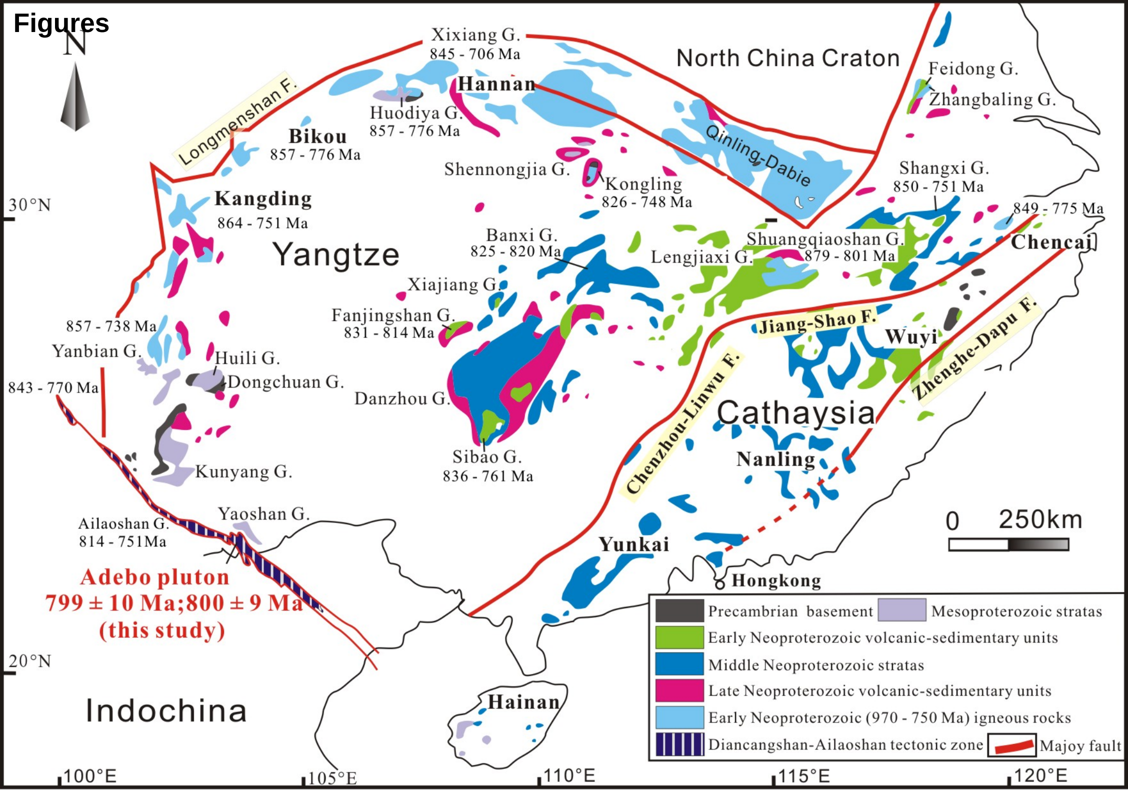

Fig.1 Y-F Cai and coauthors

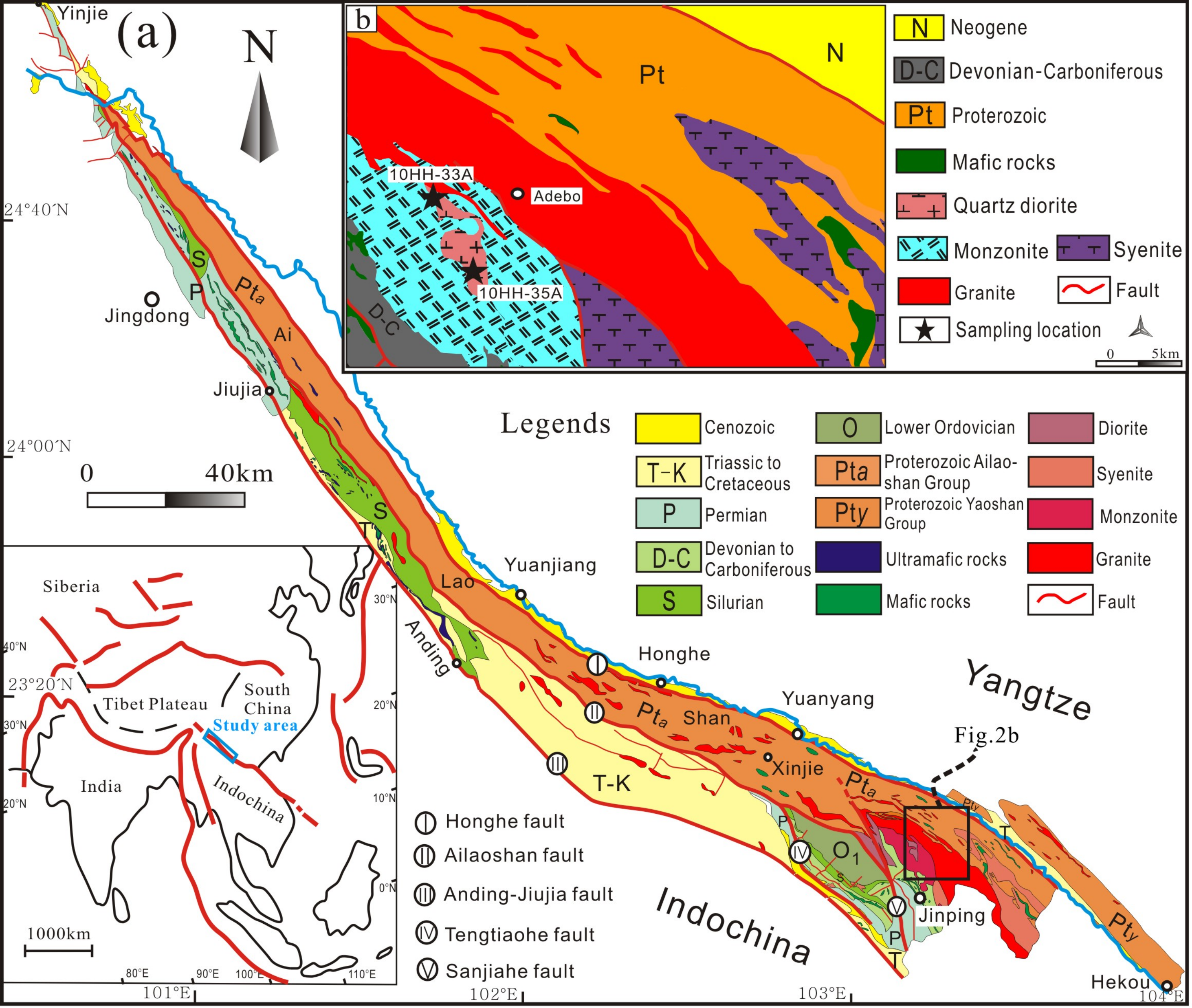

Fig.2 Y-F Cai and coauthors

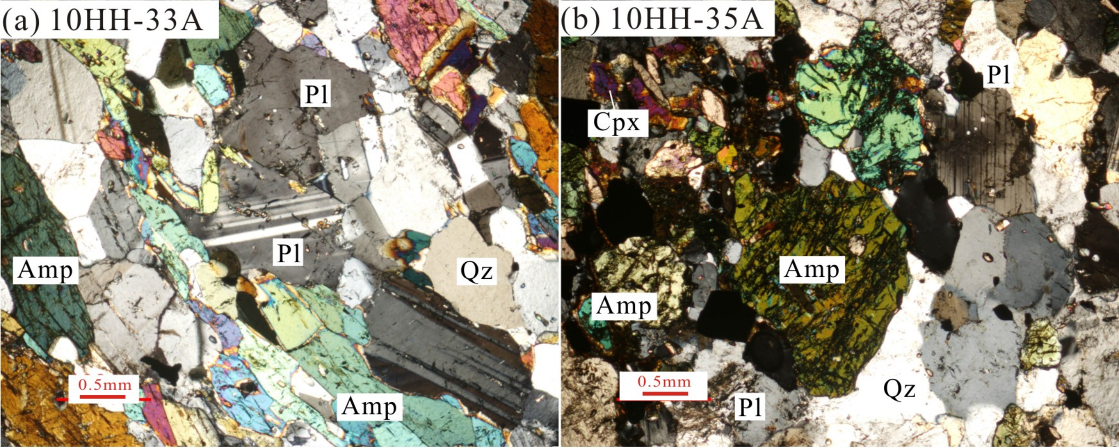

Fig.3 Y-F Cai and coauthors

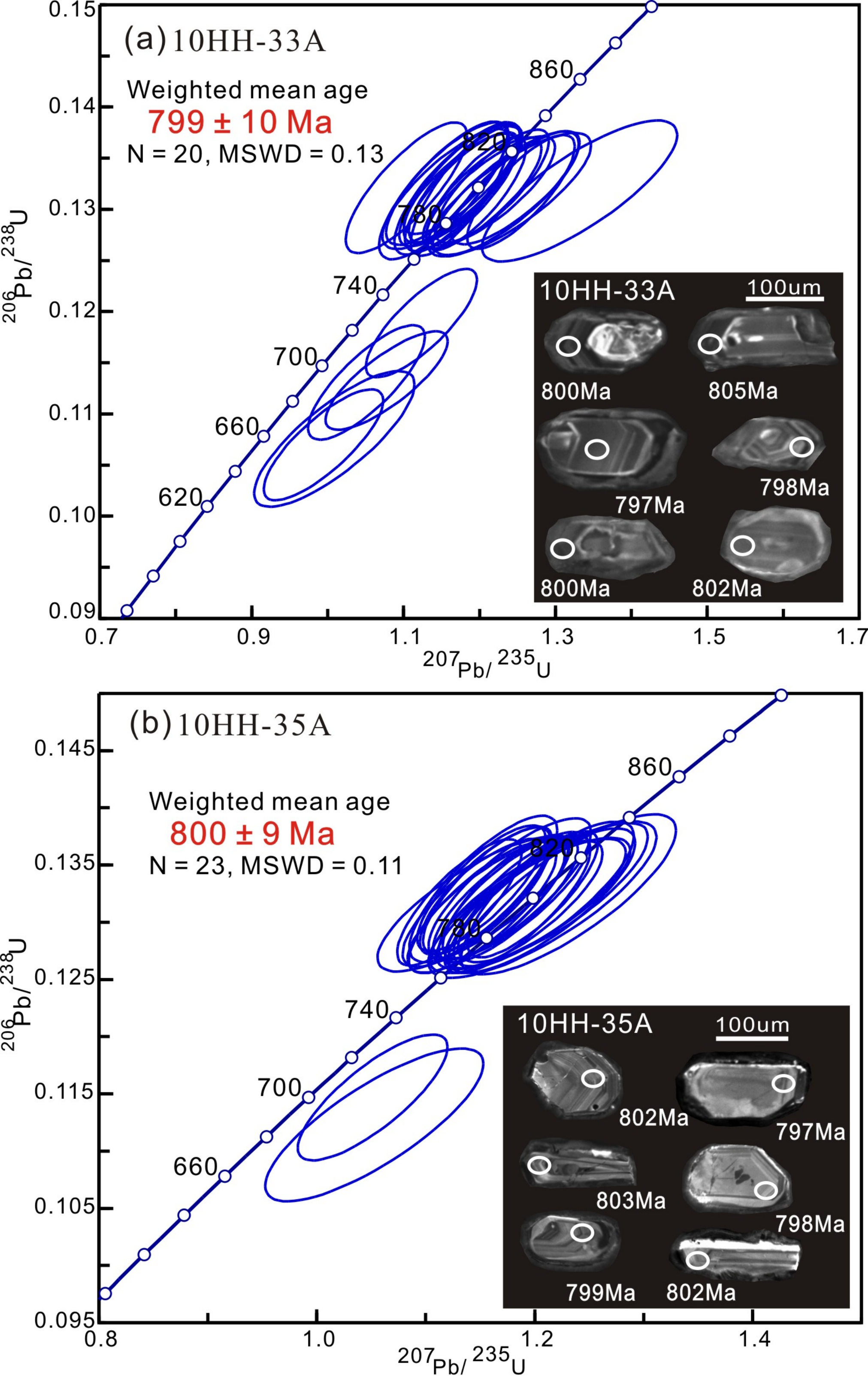

Fig.4 Y-F Cai and coauthors

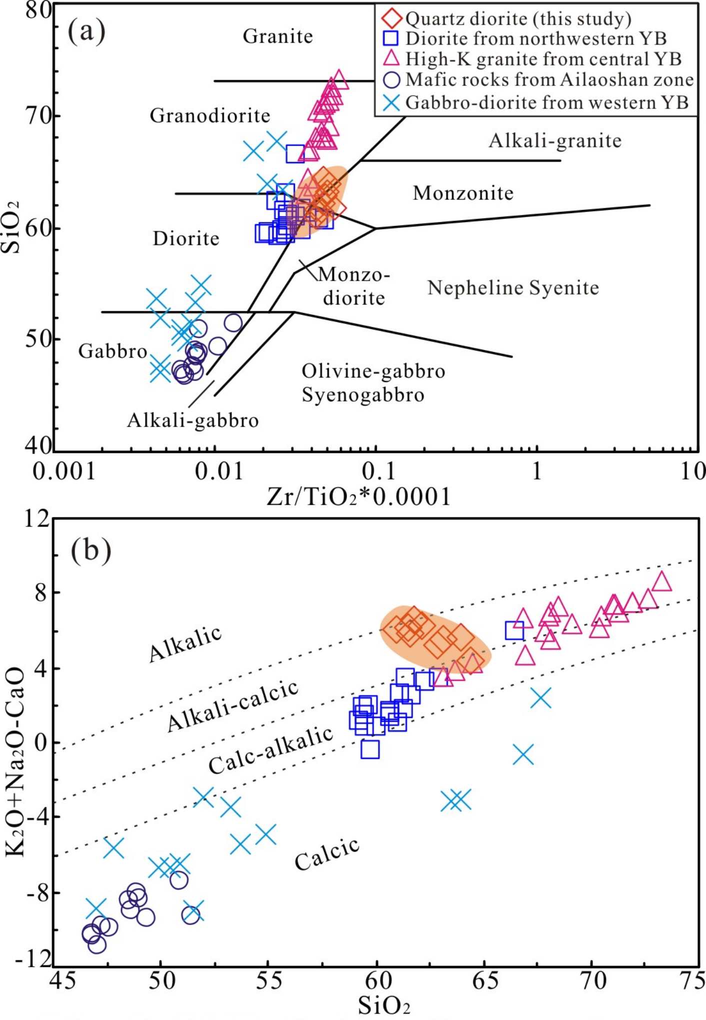

Fig.5 Y-F Cai and coauthors

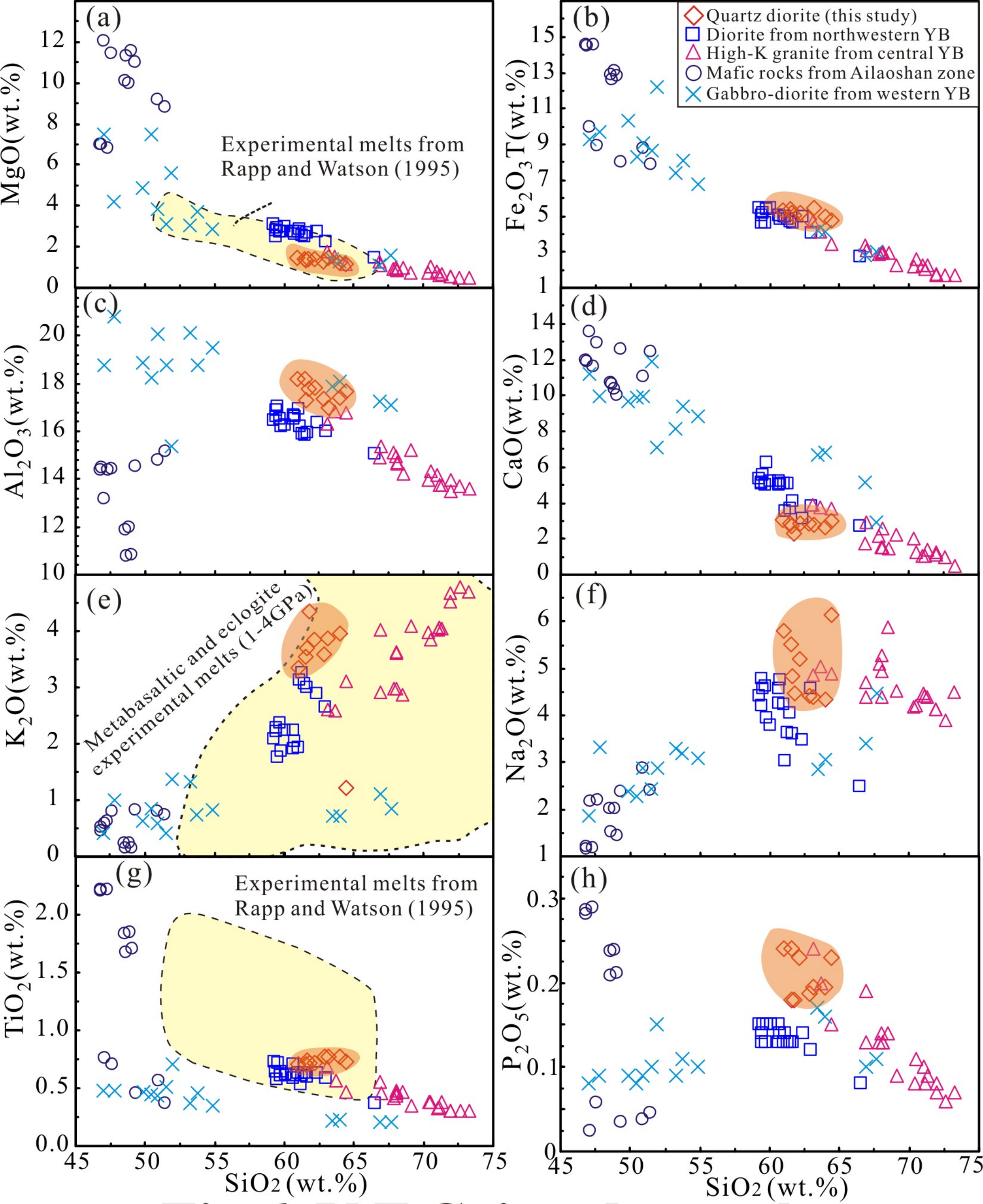

Fig.6 Y-F Cai and coauthors

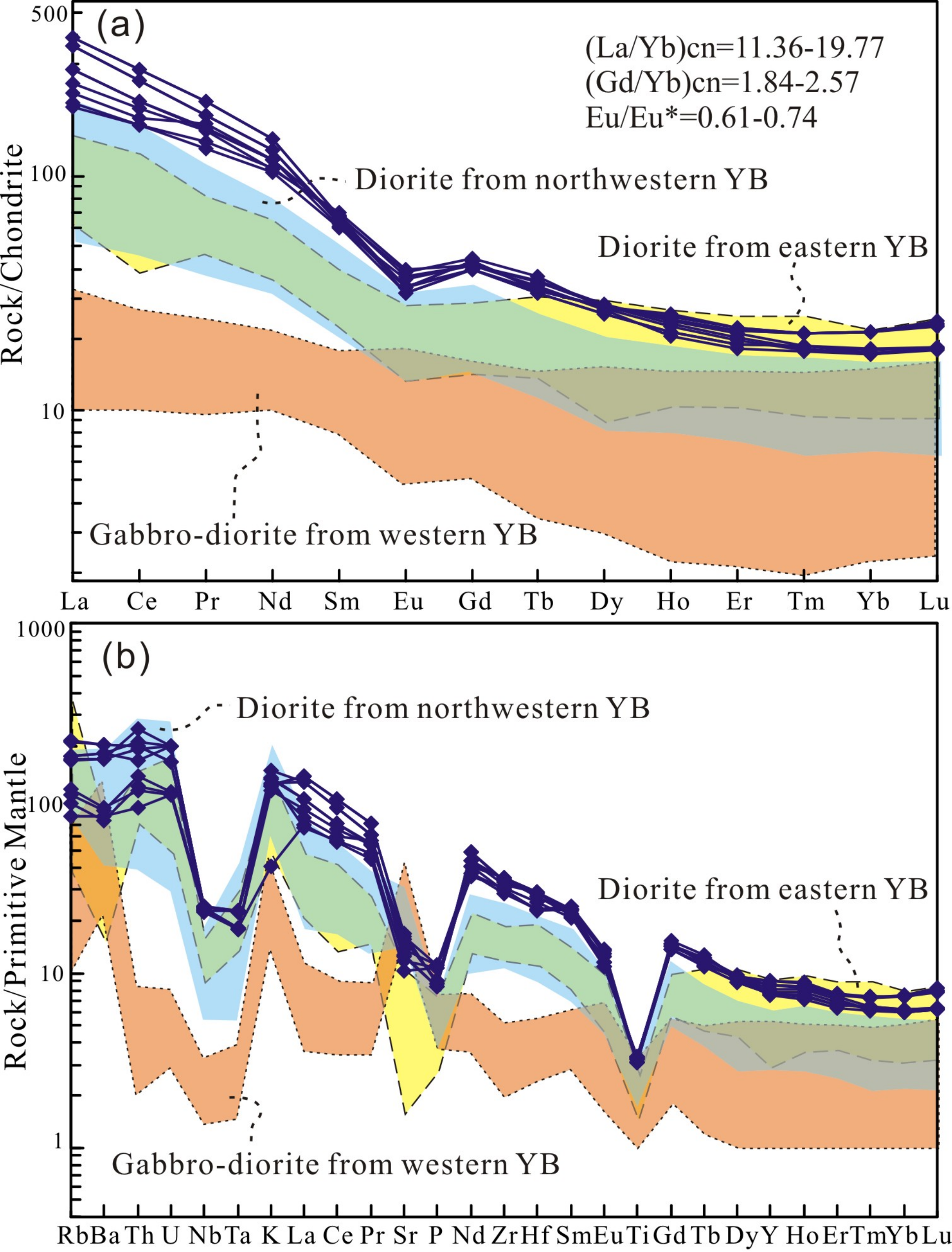

Fig.7 Y-F Cai and coauthors

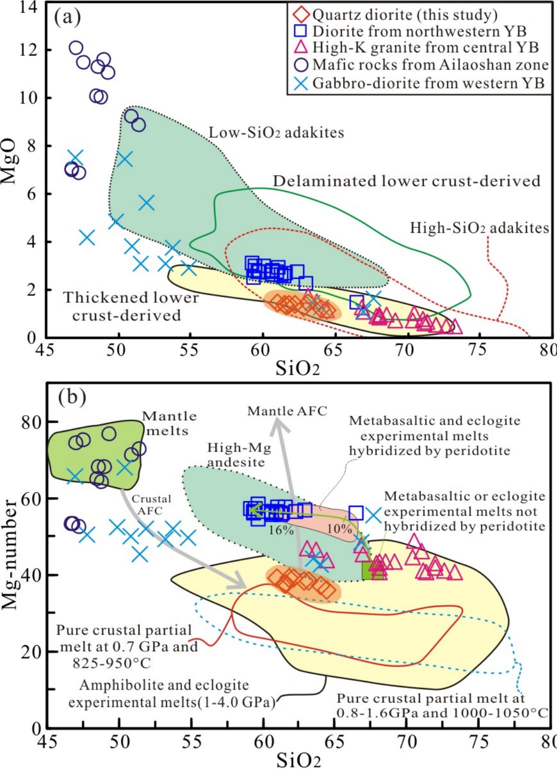

Fig.8 Y-F Cai and coauthors

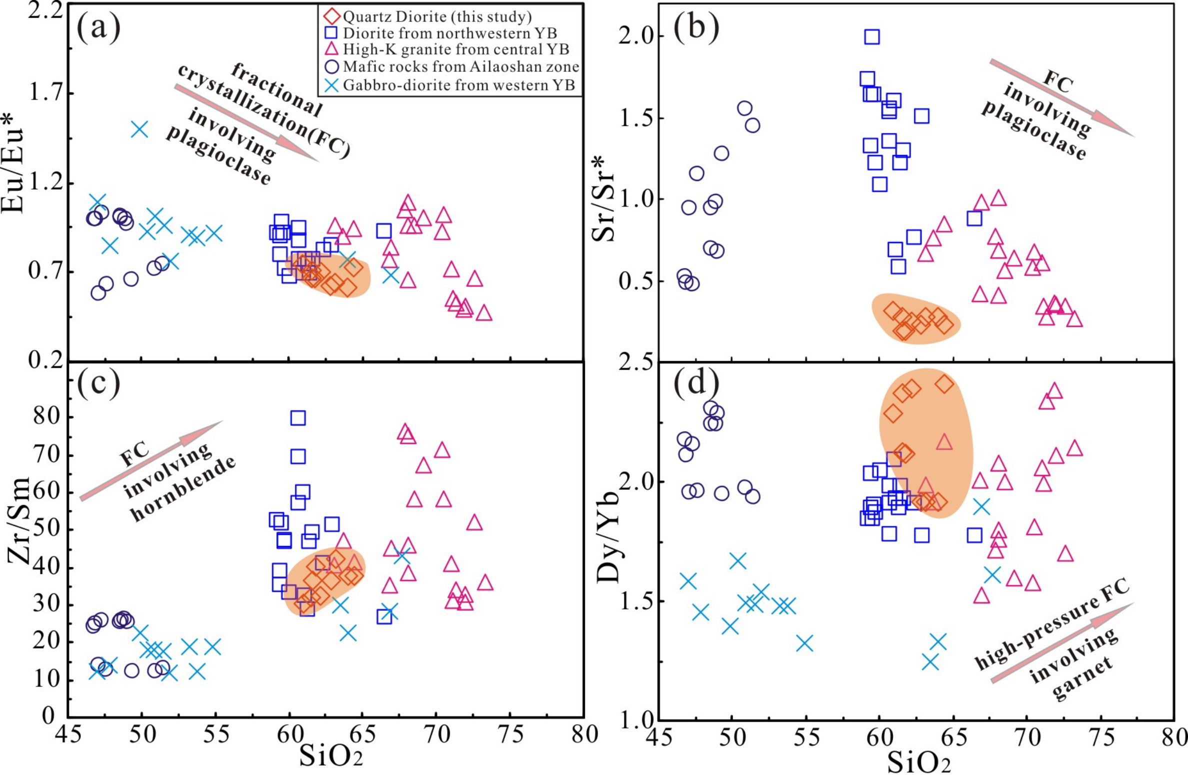

Fig.9 Y-F Cai and coauthors

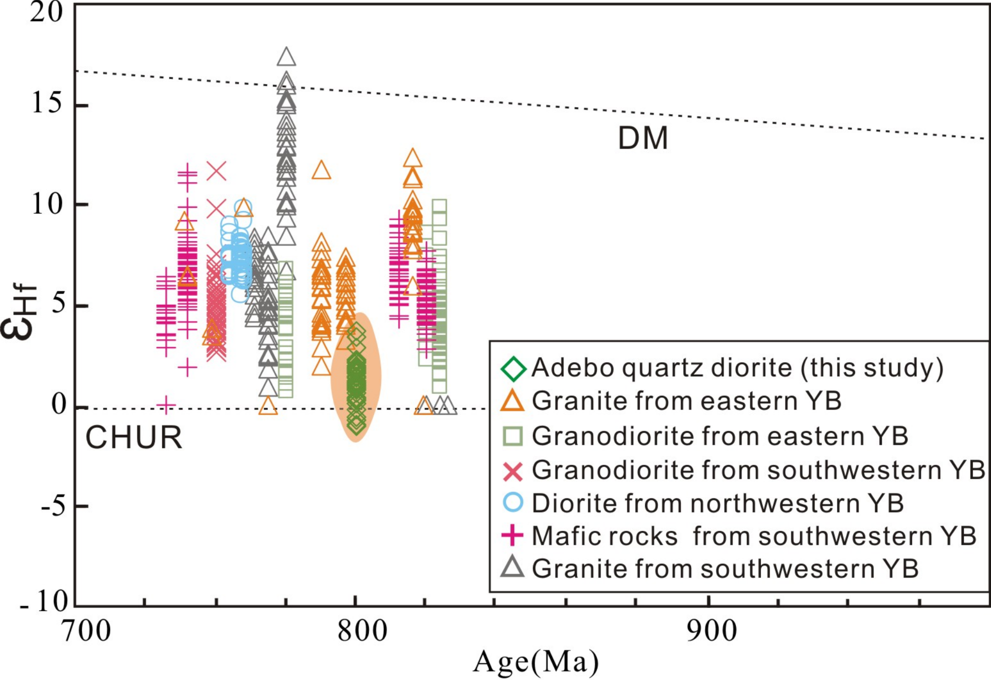

Fig.10 Y-F Cai and coauthors